Crack front instability in mixed-mode I+III: the influence of non-singular stresses

Mathias Lebihain, Jean-Baptiste Leblond, Laurent Ponson

Crack front instability in mixed-mode I+III: the influence of non-singular stresses

Mathias Lebihain[a], Jean-Baptiste Leblond[b], Laurent Ponson[b]

[a]*Laboratoire Navier, Université Gustave Eiffel, ENPC, IFSTTAR, CNRS (UMR 8205), 6-8 avenue Blaise Pascal, 77455 Marne-la-Vallée, France*
[b]*Institut Jean le Rond ∂'Alembert, Sorbonne Université, UPMC, CNRS (UMR 7190), 4 Place Jussieu, 75005 Paris, France*

Abstract

In a previous paper (Leblond et al., 2011), a theoretical instability threshold was derived for the currently observed phenomenon of crack front fragmentation under mixed-mode I+III loading conditions. Instability modes were shown to emerge when the mode mixity ratio $K^0_{\rm III}/K^0_{\rm I}$ exceeds some critical value $[K^0_{\rm III}/K^0_{\rm I}]_{\rm cr}$ that only depends on Poisson's ratio. Unfortunately, the predicted threshold was found to be much larger than that observed in general. Numerical simulations of crack front fragmentation (Chen et al., 2015), based on a phase-field model, subsequently evidenced an important role of the specimen size on the non-coplanar instability. Here, we explore theoretically the influence of existence of some finite characteristic length(s), arising from the loading, by accounting for the presence of non-singular stresses T^0_{ij} in the unperturbed configuration of the crack. By re-examining the linear stability analysis of Leblond et al. (2011) with these more general assumptions, we show that a negative non-singular stress T^0_{xx} in the direction of propagation does not affect crack front fragmentation, while a negative non-singular T^0_{zz} in the direction of the crack front strongly hampers it. On the contrary, positive non-singular stresses T^0_{xx} and T^0_{zz}, or non-zero non-singular (antiplane shear) stresses T^0_{xz}, promote the fragmentation process, sometimes through the formation of facets that drift along the front as propagation proceeds. Large values of all three of these non-singular stresses may result in a significant lowering of the threshold value $[K^0_{\rm III}/K^0_{\rm I}]_{\rm cr}$ of the mode mixity ratio for instability, even possibly down to *zero*; which stresses out the potential existence of the fragmentation instability even in pure mode I. Yet, our results cannot explain the often observed formation of non-coplanar facets at extremely low mode mixity ratios; indeed the wavelength of the instability modes predicted are comparable to the finite characteristic length(s) introduced, of at least centimetric order of magnitude, while the formation of facets has been observed experimentally at scales as low as some tens of microns.

Keywords: Brittle failure, three-dimensional fracture, configurational stability, mode I+III, non-singular stresses

1. Introduction

Crack front fragmentation is an ubiquitous phenomenon in tensile fracture of solids. It is generally observed when, in addition to the tensile mode I loading, some mode III anti-plane shear is applied. Fragmented cracks display facets that grow parallel to each other, and leave behind fracture surfaces with factory-roof-like morphologies. Since the seminal work of Sommer (1969) on glass, fragmentation patterns have been observed in nearly all types of materials, including rocks (Pollard et al., 1982), metallic alloys (Hourlier and Pineau, 1979; Eberlein et al., 2017), single crystals (Kermode et al., 2008), polymers (Knauss, 1970; Lazarus et al., 2008) and gels (Baumberger et al., 2008). In recent years, crack front fragmentation has been observed in some special materials under conditions of almost pure mode I, $K^0_{\rm I} > 0$ and $K^0_{\rm III} \simeq 0$ where $K^0_{\rm I}$ and $K^0_{\rm III}$ denote the stress intensity factors in the initial planar configuration (Lin et al., 2010; Ronsin et al., 2014; Vasudevan, 2018; Kolvin et al., 2018). This suggests that mode I crack configurations in these materials may be bi-stable, either simple or faceted.

Despite the ubiquity of crack fragmentation during failure of materials, a comprehensive understanding of, and a fully predictive criterion for, the transition of a propagating crack from a smooth surface to a fragmented one is still missing. LEFM (linear elastic fracture mechanics), applied to slightly perturbed cracks, has proved to be the most promising theoretical framework to describe and predict the phenomenon. In their pioneering work, Leblond et al. (2011), inspired by the results of Pons and Karma (2010)'s numerical simulations based on a phase-field-model, showed that helical perturbations to an initially straight crack front may grow without bound, if the mode mixity ratio $K^0_{\rm III}/K^0_{\rm I}$ exceeds some critical value $[K^0_{\rm III}/K^0_{\rm I}]^{\rm ref}_{\rm cr}$, that only depends on Poisson's ratio. It was then shown by Chen et al. (2015) that such a bifurcation is subcritical, so that fragmented crack fronts may exist even at *low* mixity ratios $K^0_{\rm III}/K^0_{\rm I} \ll 1$, and so may co-exist with planar crack surfaces under the same loading conditions. However, such a scenario does not account for the emergence of facets in propagating cracks at *extremely low* levels of anti-plane shear, $K^0_{\rm III}/K^0_{\rm I} \ll 1$ (very much lower than the theoretical value $[K^0_{\rm III}/K^0_{\rm I}]^{\rm ref}_{\rm cr}$), which have been reported in brittle polymers and gels (Lin et al., 2010; Ronsin et al., 2014; Vasudevan, 2018; Kolvin et al., 2018).

To reconcile the onset of instability predicted by LEFM and the (material dependent) threshold observed experimentally, Leblond et al. (2019) and Vasudevan et al. (2020) investigated

*Corresponding author : mathias.lebihain@enpc.fr

the effect of a mode-dependent fracture energy, and showed that such a dependence may dramatically lower the fragmentation threshold, provided that the shear-mode-dependence of G_c is strong enough. Last but not least, they also showed that in the presence of some additional global mode II component, $K_{II}^0 \neq 0$, facets can gradually drift along the crack front as it propagates, a behavior which is indeed observed experimentally (Lin et al., 2010; Ronsin et al., 2014; Vasudevan, 2018; Kolvin et al., 2018).

The role of the presence of some finite characteristic lengths, arising from the finite dimensions of the structure and/or the spatial variation of the loading, upon the fragmentation instability has been largely neglected so far. However numerical simulations of crack front fragmentation, based on a phase-field model, have shown that reducing the specimen size results in a significant decrease of the instability threshold (Chen et al., 2015). In addition, theoretical investigations of the effect of non-singular stresses T_{xx}^0 (parallel to the direction of propagation), T_{zz}^0 (parallel to the crack front) and T_{xz}^0 (simple shear in the crack plane), due to Cotterell and Rice (1980), Gao (1992) and Xu et al. (1994), have shown that large values of these quantities may favor out-of-plane crack excursions, even under pure more I conditions. The presence of such non-singular stresses in the unperturbed configuration of the crack is intimately tied to the presence of one or several finite characteristic lengths.

In this work, we explore theoretically the role of the presence of some finite characteristic lengths upon the fragmentation instability. These lengths, naturally defined as $\mathcal{L}_{ij} = (K_I^0/T_{ij}^0)^2$ where T_{ij}^0 denotes any of the three non-singular stresses T_{xx}^0, T_{zz}^0, T_{xz}^0, will arise only from the spatial variation of the loading, in the absence of any characteristic length in the infinite model-geometry considered. The structural length scales $\mathcal{L}_{ij}$ may interact with the length scale characterizing the unstable mode of crack propagation, as shown in a broader context by Favier et al. (2006); Vasoya et al. (2016). We shall thus seek to determine the impact of the presence of some non-singular stresses, or equivalently some length scales $\mathcal{L}_{ij}$, upon the transition from a planar to a fragmented crack; and whether or not this presence may explain the low fragmentation threshold observed in some fracture experiments. We shall also explore the effect of non-singular stresses upon the morphology of the facets, and in particular (i) their possible drift along the crack front, and (ii) the possible selection of the characteristic size of the facets at the fragmentation threshold.

The paper is organized as follows:

- In Section 2, we first provide the expressions of the local variations δK_I, δK_{II}, δK_{III} of the stress intensity factor along a perturbed crack front, under mixed mode I+III loading conditions with additional non-singular stresses T_{xx}^0, T_{zz}^0 and T_{xz}^0.

- These expressions are then applied in Section 3 to predict the fragmentation threshold and the properties of instability modes. The derivation is based on the assumption that both Goldstein and Salganik (1974)'s principle of local symmetry and Griffith (1921)'s energetic condition are satisfied at all instants and all positions along the front, .

- The impact of non-singular stresses upon the fragmentation instability is analyzed in depth in Section 4.

- Finally Section 5 presents a synthesis of our main findings and their application to experimental situations.

2. First-order order perturbation of a semi-infinite crack in an infinite body

2.1. Unperturbed geometry and loading - Generalities

We consider a semi-infinite crack embedded in an infinite body made of some isotropic linearly elastic material. In the initial reference configuration Γ, the crack is planar and its front is straight (see Fig. 1a). We adopt the usual convention of LEFM, and thus use a Cartesian frame $Oxyz$ with origin O chosen arbitrarily within the crack plane, axis (Ox) parallel to the direction of crack propagation, (Oy) parallel to the direction orthogonal to the crack plane, and (Oz) parallel to the crack front (see Fig. 1a). The associated unit vectors are denoted $(\mathbf{e}_x, \mathbf{e}_y, \mathbf{e}_z)$. In the following, the notations $f_{,x}$, $f_{,y}$, $f_{,z}$ denote the partial derivatives of the function f with respect to the coordinates x, y, z.

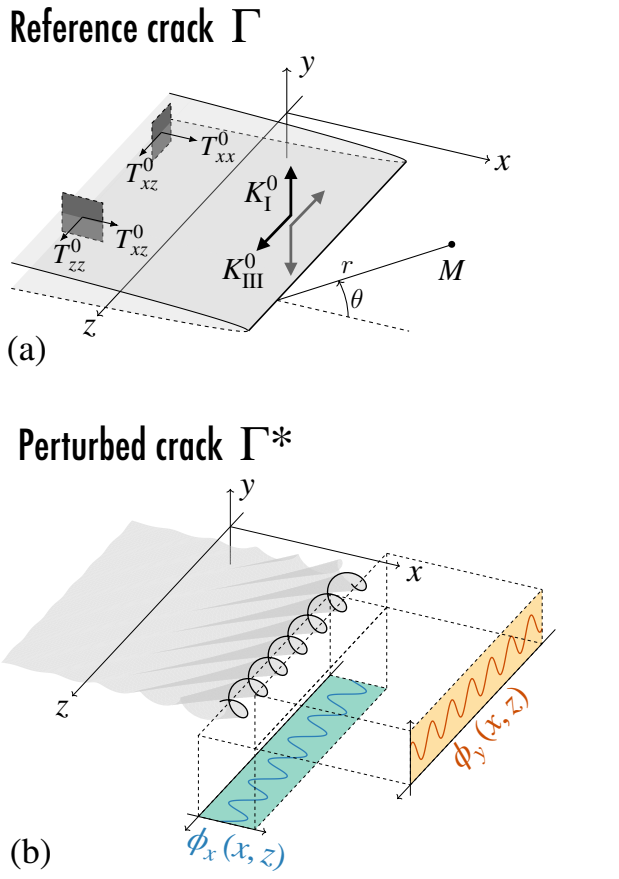

Figure 1: (a) The reference semi-infinite crack Γ with a straight front is loaded in mixed-mode I+III with non-zero non-singular stresses. (b) The crack front and its surface are perturbed both within and out of the original plane, by small amounts noted ϕ_x and ϕ_y respectively.

The unperturbed crack is loaded under mixed-mode I+III conditions through some system of forces, such that the unperturbed SIFs $K_{\rm I}^0$ and $K_{\rm III}^0$ be independent of the position x of the crack front and the position z of their point of observation within this front. The SIF $K_{\rm III}^0$ may harmlessly be assumed to be non-negative. In addition the unperturbed stress field is characterized by non-singular stresses $(T_{xx}^0, T_{xz}^0, T_{zz}^0)$ also independent of x and z. These non-singular stresses correspond to the constant terms in the asymptotic expansion of the stress field in the vicinity of the crack front, that reads (Williams, 1952):

$$\begin{cases} \sigma_{xx}^0(r,\theta) = \dfrac{K_{\rm I}^0}{\sqrt{2\pi r}} \cos\left(\frac{\theta}{2}\right)\left[1 - \sin\left(\frac{\theta}{2}\right)\sin\left(\frac{3\theta}{2}\right)\right] + T_{xx}^0 + O(r^{1/2}) \\ \sigma_{yy}^0(r,\theta) = \dfrac{K_{\rm I}^0}{\sqrt{2\pi r}} \cos\left(\frac{\theta}{2}\right)\left[1 + \sin\left(\frac{\theta}{2}\right)\sin\left(\frac{3\theta}{2}\right)\right] + O(r^{1/2}) \\ \sigma_{xy}^0(r,\theta) = \dfrac{K_{\rm I}^0}{\sqrt{2\pi r}} \cos\left(\frac{\theta}{2}\right)\sin\left(\frac{\theta}{2}\right)\cos\left(\frac{3\theta}{2}\right) + O(r^{1/2}) \\ \sigma_{xz}^0(r,\theta) = -\dfrac{K_{\rm III}^0}{\sqrt{2\pi r}} \sin\left(\frac{\theta}{2}\right) + T_{xz}^0 + O(r^{1/2}) \\ \sigma_{yz}^0(r,\theta) = \dfrac{K_{\rm III}^0}{\sqrt{2\pi r}} \cos\left(\frac{\theta}{2}\right) + O(r^{1/2}) \\ \sigma_{zz}^0(r,\theta) = 2\nu\dfrac{K_{\rm I}^0}{\sqrt{2\pi r}} \cos\left(\frac{\theta}{2}\right) + T_{zz}^0 + O(r^{1/2}) \end{cases} \tag{1}$$

where (r,θ) denote the polar coordinates of the point of observation M in the local plane orthogonal to the crack front (see Fig. 1a), and ν Poisson's ratio. The non-singular stresses T_{ij}^0 typically emerge from the finite dimensions defined by the loading, in the absence of any characteristic length defined by the geometry itself. Their magnitudes $|T_{ij}^0|$ define some characteristic lengths

$$\mathcal{L}_{ij} = \left(\frac{K_{\rm I}^0}{T_{ij}^0}\right)^2 \tag{2}$$

that describe the spatial extent of a $K_{\rm I}$-dominated zone where the terms in $K_{\rm I}^0$ of Eq. (1) prevail over those in T_{ij}^0.

2.2. First-order expressions of the stress intensity factors along the crack front in a slightly perturbed configuration

In a perturbed configuration Γ^*, the crack front is displaced within the original crack plane by a small amount $\phi_x(x,z)$ in the direction (Ox), and the crack surface is displaced out of the original crack plane by a small amount $\phi_y(x,z)$ in the direction (Oy) (see Fig. 1.b); the argument x here represents the average position of the perturbed crack front in the direction of propagation, in the first function, and the first coordinate of the point of observation of the out-of-plane perturbation, in the second.

The p-th SIF $K_{\rm p}$ can be expressed as the sum of the SIF $K_{\rm p}^0$ associated to the reference configuration Γ, and the perturbation $\delta K_{\rm p}$ arising from the displacements of the crack front and surface:

$$K_{\rm p}(x,z) = K_{\rm p}^0 + \delta K_{\rm p}(x,z). \tag{3}$$

Furthermore because of linearity, each SIF perturbation $\delta K_{\rm p}$ can be decomposed as the sum of a term $\delta_K K_{\rm p}$ resulting from the macroscopic mixed-mode I+III loading, and a term $\delta_T K_{\rm p}$ resulting from the presence of non-zero non-singular stresses:

$$\delta K_{\rm p}(x,z) = \delta_K K_{\rm p}(x,z) + \delta_T K_{\rm p}(x,z) \tag{4}$$

The detailed expressions of the perturbations $\delta_K K_{\rm p}$ and $\delta_T K_{\rm p}$ are provided in the works of Gao and Rice (1986) for the in-plane perturbation ϕ_x, and Movchan et al. (1998) for the out-of-plane perturbation ϕ_y; they are given in Eqs (A.1) and (A.9) of Appendix A respectively. Some simplifications have been made here according to the following hypotheses:

1. The characteristic length defined by the spatial variations of the loading is supposed to be much larger than the typical distances of variation of the perturbations $\phi_x(x,z)$ and $\phi_y(x,z)$ of the crack front and surface. (This is the assumption that permits to consider the K_p^0's and T_{ij}^0's as independent of x).
2. The characteristic length associated to the coefficients $A_{\rm q}$ appearing in the terms proportional to $r^{1/2}$ in Eq. (1) – of the order of $K_{\rm p}/A_{\rm q}$ – is much larger than the lengths $\mathcal{L}_{ij}$ associated to the non-singular stresses.

It is worth noting here that:

1. The expressions of the variations $\delta_K K_{\rm p}$ involve three types of terms: *local* terms that relate to the local crack front orientation defined by the derivatives $\phi_{i,j}$, *semi-local* terms that involve integrals of the displacements ϕ_i along the whole crack front, and fully *non-local* terms that contain integrals of the displacements ϕ_i over the entire crack surface.
2. The variations SIFs $\delta_T K_{\rm p}$ were derived by Movchan et al. (1998) only for a sinusoidal perturbation $\phi_y(z) = A\cos(kz)$ independent of x. Their expressions for an arbitrary perturbation $\phi_y(x,z)$ are derived in Appendix A.
3. The variations $\delta_T K_{\rm p}$ involve only non-local terms related to the "morphology" of the crack surface, in Movchan et al. (1998)'s terminology.

3. Linear stability analysis of coplanar propagation

3.1. Generalities

Like in our previous works (Leblond et al., 2011, 2019; Vasudevan et al., 2020), we are looking for configurations of the crack and its front (ϕ_x, ϕ_y) other than the trivial one (planar crack with straight front), satisfying a "double" propagation criterion enforced at all points of the crack front and all instants of propagation. This criterion consists of:

- Goldstein and Salganik (1974)'s principle of local symmetry, stipulating that the local SIF $K_{\rm II}(x,z)$ of mode II must be zero;
- Griffith (1921)'s criterion $G(x,z) = G_{\rm c}$, which states that the local energy release rate $G(x,z)$ must be equal to the local fracture energy $G_{\rm c}$, assumed here to be uniform.[1]

[1] It is interesting to note here that the validity of Griffith (1921)'s criterion at small scales, that is in its *local* form $G(x,z) = G_{\rm c}$, was recently tested experimentally by Wang et al. (2022) by investigating the balance of energy during the tensile failure of a brittle gel.

The analysis will be based on the consideration of instability modes associated with perturbations of the crack front and surface of the following form (Vasudevan et al., 2020):

$$\begin{cases} \phi_x(x,z) = \mathrm{Re}\left[e^{\lambda x}\psi_x(z)\right] \\ \phi_y(x,z) = \mathrm{Re}\left[e^{\lambda x}\psi_y(z)\right] \end{cases} \quad (5)$$

where λ is the *complex growth rate* of the mode, and $\psi_x(z)$ and $\psi_y(z)$ two unknown complex functions. Instability of coplanar propagation is characterized by the condition $\mathrm{Re}(\lambda) > 0$. Also, as noted by (Vasudevan et al., 2020) and briefly re-explained below, a non-zero imaginary part of λ indicates *a drifting motion of the instability mode along the crack front as it propagates*.

Use will be made of Fourier transforms in the direction z of the crack front. The definition adopted here for the Fourier transform $\hat{\chi}(k)$ of an arbitrary function $\chi(z)$ is:

$$\hat{\chi}(k) = \frac{1}{2\pi}\int_{-\infty}^{+\infty} \chi(z) e^{-ikz} dz \;\Leftrightarrow\; \chi(z) = \int_{-\infty}^{+\infty} \hat{\chi}(k) e^{ikz} dk. \quad (6)$$

One can see here that the imaginary part of λ governs the drifting motion of instability modes: indeed writing λ as $\lambda_1 + i\lambda_2$ with real λ_1 and λ_2, one sees that the expressions of the perturbations ϕ_x and ϕ_y involve, for each Fourier component, the factor $e^{\lambda x}e^{ikz} = e^{\lambda_1 x}e^{i(\lambda_2 x + kz)}$ depicting an exponential growth combined with a "drift velocity" $dz/dx = -\lambda_2/k$ - see (Vasudevan et al., 2020) for details.

For each Fourier component, we define a *normalized complex growth rate* ξ by the formula

$$\xi = \lambda/|k|. \quad (7)$$

This dimensionless ratio compares the complex growth rate λ of the perturbations in the direction x of propagation to their wavenumber $|k|$ in the direction z of the crack front. The value of ξ is restricted to the half-plane $\mathrm{Re}(\xi) > -1$ for convergence of the integrals in Eqs. (A.1) and (A.9), which provide the variations of the SIFs due to the perturbations of the crack front and surface. Note also that the imaginary part of ξ is directly connected to the angle α characterizing the drifting motion of the mode (see the inset of Fig.3.b) through the relation

$$\alpha = \arctan\left[-\mathrm{Im}(\xi)\right]. \quad (8)$$

The next two sections aim at deriving the condition on ξ that results from the double propagation criterion, when the crack is loaded in mixed-mode I+III with additional non-zero non-singular stresses. This will permit, upon examination of the real and imaginary parts of ξ, to discuss both the conditions governing instability of coplanar propagation, and the possible drifting motion of instability modes.

3.2. Application of the principle of local symmetry

We first make use of Goldstein and Salganik (1974)'s principle of local symmetry, stipulating that the stress intensity factor of mode II must be uniformly zero at all points of the crack front and all instants. In the absence of macroscopic mode II ($K_{\mathrm{II}}^0 = 0$), this condition reduces to:

$$\delta K_{\mathrm{II}}(x,z) = 0 \quad (9)$$

The expression of δK_{II} displayed in Eqs. (A.1) and (A.9) involves complex integrals of the perturbations (ϕ_x, ϕ_y) over the entire crack front and the entire crack surface. Fortunately, these integrals take a rather "simple" form when expressed in Fourier's space, for instabilities of the type considered in Eq. (5). The expressions of the variations $\widehat{\delta_K K_{\mathrm{p}}}$ related to the unperturbed SIFs were derived by Leblond et al. (2019), and are recalled in Eq. (B.1) of Appendix B.a. The expressions of the variations $\widehat{\delta_T K_{\mathrm{p}}}$ associated to the unperturbed non-singular stresses are derived in Appendix B.b, and given in Eq. (B.4).

Inserting Eqs. (B.1) and (B.4) in (9) yields, for every wavenumber k:

$$4i\rho_0 s\,\hat{\psi}_x(k) = \hat{\psi}_y(k)\left\{2 - 3\nu + (2-\nu)\xi - \frac{2\sqrt{2}}{(\xi+1)^{3/2}}\left[((2-\nu)\xi + 2)\,\xi q_{xx}^0 + \nu q_{zz}^0 + 2is\,((1-\nu)\xi + 1)\,q_{xz}^0\right]\right\}. \quad (10)$$

In this equation the quantity

$$\rho_0 = \frac{K_{\mathrm{III}}^0}{K_{\mathrm{I}}^0} \quad (\geq 0) \quad (11)$$

denotes the unperturbed mixity ratio, s the sign of the wavenumber k, and the quantities

$$q_{ij}^0 = \frac{T_{ij}^0}{\sqrt{|k|}K_{\mathrm{I}}^0} = \frac{\epsilon_{ij}}{\sqrt{|k|\mathcal{L}_{ij}}} \quad , \quad \epsilon_{ij} = \mathrm{sgn}(T_{ij}^0) \quad (12)$$

are related to the ratios of the wavelength $\ell_{\mathrm{pert}} = 2\pi/|k|$ of the perturbations to the lengthscales $\mathcal{L}_{ij}$ set by the non-singular stresses T_{ij}, and defined by Eq. (2).

3.3. Application of Griffith's criterion

We now use Griffith (1921)'s criterion, which states that the crack propagates when the local energy release rate $G(x,z)$ is equal to the local fracture energy G_{c}. We consider here the case where the field of fracture energy G_{c} is uniform. Then necessarily

$$\delta G(x,z) = 0 \quad (13)$$

at all points of the crack front and all instants.

The energy-release-rate may be calculated from the SIFs using Irwin (1958)'s well-known formula:

$$G(x,z) = \frac{1-\nu^2}{E}\left[K_{\mathrm{I}}^2(x,z) + K_{\mathrm{II}}^2(x,z)\right] + \frac{1+\nu}{E}K_{\mathrm{III}}^2(x,z) \quad (14)$$

where E denotes Young's modulus. The first-order contribution of the perturbations ϕ_x, ϕ_y of the crack front and surface to the energy-release-rate reads:

$$\delta G(x,z) = 2\frac{1-\nu^2}{E}K_{\mathrm{I}}^{0\,2}\left[\frac{\delta K_{\mathrm{I}}(x,z)}{K_{\mathrm{I}}^0} + \frac{\rho_0}{1-\nu}\frac{\delta K_{\mathrm{III}}(x,z)}{K_{\mathrm{I}}^0}\right]. \quad (15)$$

Griffith (1921)'s criterion (Eq. (13)) then yields:

$$\delta K_{\mathrm{I}}(x,z) + \frac{\rho_0}{1-\nu}\delta K_{\mathrm{III}}(x,z) = 0. \quad (16)$$

Inserting Eqs. (B.1) and (B.4) into (16) yields for every wavenumber k:

$$\begin{aligned}\left[(1-\nu)(2-\nu)+(2+\nu)\rho_0^2\right]\hat{\psi}_x(k) \\ = 2i\rho_0 s\,\hat{\psi}_y(k)\left\{-2(1-\nu)+\frac{(1-2\nu)(2-\nu)}{\sqrt{2(\xi+1)}}\right. \\ +\frac{\sqrt{2}}{\sqrt{\xi+1}}\left[\nu\frac{\xi}{\xi+1}q^0_{xx}-\left(2-\nu-\frac{\nu}{\xi+1}\right)q^0_{zz}\right. \\ \left.\left.+is\left((2-\nu)\xi-\nu\frac{\xi-1}{\xi+1}\right)q^0_{xz}\right]\right\}. \end{aligned} \tag{17}$$

3.4. *Combination of the two parts of the criterion*

Combination of Eqs.(10) and (17) yields:

$$F(\rho_0,\xi)+f_{xx}(\rho_0,\xi)q^0_{xx}+f_{zz}(\rho_0,\xi)q^0_{zz}+isf_{xz}(\rho_0,\xi)q^0_{xz}=0 \tag{18}$$

where

$$\left\{\begin{array}{rcl} F(\rho_0,\xi) & = & (1-\nu)(2-3\nu)-3(2-\nu)\rho_0^2 \\ & & +\left[(1-\nu)(2-\nu)+(2+\nu)\rho_0^2\right]\xi \\ & & +4\dfrac{\sqrt{2}}{\sqrt{\xi+1}}(1-2\nu)\rho_0^2 \\ f_{xx}(\rho_0,\xi) & = & -\dfrac{2\sqrt{2}\xi}{(\xi+1)^{3/2}}\left[(1-\nu)\left((2-\nu)\xi+2\right)\right. \\ & & \left.+\left((2+\nu)\xi+2\right)\rho_0^2\right] \\ f_{zz}(\rho_0,\xi) & = & -\dfrac{2\sqrt{2}}{(\xi+1)^{3/2}}\left[\nu(1-\nu)+(4\xi+4-\nu)\rho_0^2\right] \\ f_{xz}(\rho_0,\xi) & = & -\dfrac{4\sqrt{2}}{(\xi+1)^{3/2}}\left[(1-\nu)\left((1-\nu)\xi+1\right)\right. \\ & & \left.-\left(2\xi^2+(1-\nu)\xi-1\right)\rho_0^2\right] \end{array}\right. \tag{19}$$

Equation (18) implicitly defines the value of the normalized growth rate ξ for a given set of loading parameters $(\rho_0, q^0_{xx}, q^0_{xz}, q^0_{zz})$; our interest is in values of ξ having a positive real part, corresponding to exponentially growing perturbations. The values of ξ satisfying Eq. (18) can be computed numerically relatively easily, this equation being equivalent to a polynomial equation of the fifth degree in the variable $\zeta = 1/\sqrt{\xi+1}$. The numerical procedure is described in Appendix C.

It is worth noting that in the absence of non-singular stresses T^0_{ij}, Eq. (18) reduces to condition (20) of Leblond et al. (2011) assessing configurational stability in mixed-mode I+III.

4. Influence of non-singular stresses on the configurational stability of a plane crack

4.1. *The stability analysis of Leblond et al. (2011) without non-singular stresses*

We first consider the *reference case* of mixed mode I+III in the absence of non-singular stresses, which corresponds to the situation examined by Leblond et al. (2011). They showed that – for values of Poisson's ratio greater than $\nu_c \approx 0.03$ – admissible solutions are found along the real line $\mathrm{Im}(\lambda) = 0$, so that no drift of instability modes is predicted. Moreover, the growth rate $\mathrm{Re}(\lambda) = \lambda$ is negative (decaying perturbations) for low values of the mode mixity ratio $\rho^0 = K^0_{\mathrm{I}}/K^0_{\mathrm{III}}$, but becomes positive (increasing perturbations) for ratios larger than some critical value $[K^0_{\mathrm{III}}/K^0_{\mathrm{I}}]^{\mathrm{ref}}_{\mathrm{cr}}$. Both this critical value, and the evolution of $\mathrm{Re}(\lambda) = \lambda$ with $K^0_{\mathrm{I}}/K^0_{\mathrm{III}}$, depend on Poisson's ratio ν. In particular, the value of $[K^0_{\mathrm{III}}/K^0_{\mathrm{I}}]^{\mathrm{ref}}_{\mathrm{cr}}$ is given by

$$[K^0_{\mathrm{III}}/K^0_{\mathrm{I}}]^{\mathrm{ref}}_{\mathrm{cr}} = \sqrt{\frac{(1-\nu)(2-3\nu)}{3(2-\nu)-4\sqrt{2}(1-2\nu)}} \tag{20}$$

The results of the stability analysis are given in Fig. 2 for $\nu = 0.3$, in the form of a plot of the "reduced" growth rate $\mathrm{Re}(\lambda)/|k| = \lambda/|k|$ versus the mixity ratio $\rho^0 = K^0_{\mathrm{I}}/K^0_{\mathrm{III}}$. For the value of ν considered, $[K^0_{\mathrm{III}}/K^0_{\mathrm{I}}]^{\mathrm{ref}}_{\mathrm{cr}} \simeq 0.52$. (As noted by Leblond et al. (2011), another branch of solutions exists near $\mathrm{Re}(\lambda) \simeq -1$, but it corresponds to exponentially decaying perturbations of little interest).

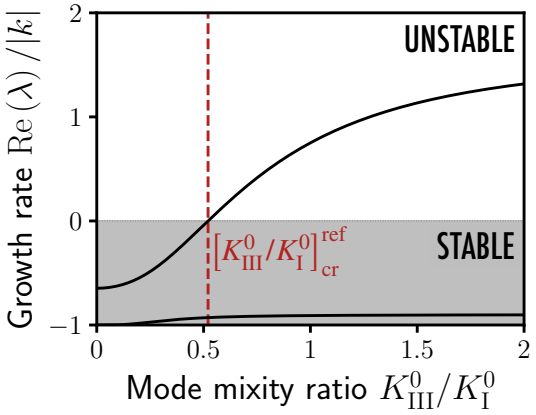

Figure 2: Leblond et al. (2011)'s configurational stability analysis of a planar crack loaded on mode I+III, for a Poisson ratio $\nu = 0.3$: when the mode mixity ratio $K^0_{\mathrm{III}}/K^0_{\mathrm{I}}$ is larger than some critical value $[K^0_{\mathrm{III}}/K^0_{\mathrm{I}}]_{\mathrm{cr}}$ (vertical red line), the perturbations grow exponentially ($\mathrm{Re}(\lambda) > 0$), whatever their wavelength ℓ_{pert}.

Yet, in phase-field simulations of brittle fracture (Pons and Karma, 2010; Chen et al., 2015) or experiments of crack initiation in mixed mode I+III (Lin et al., 2010; Pham and Ravi-Chandar, 2014), non-zero non-singular stresses are bound to emerge from the finiteness of the crack dimensions with respect to the size of the fracture specimen, and from the boundary conditions. We shall now extend the study of Leblond et al. (2011) by building on equation (18) to explore the influence of such non-singular stresses upon the stability of the planar configuration of the crack.

4.2. *Influence of T^0_{xx}*

We first explore the influence of T^0_{xx}. The sign ϵ_{xx} of this non-singular stress has been shown to control the stability of the crack path in both 2D (Cotterell and Rice, 1980) and 3D situations (Gao, 1992; Xu et al., 1994), positive values of T^0_{xx} being associated with instability. However to the best of the authors' knowledge, the influence of T^0_{xx} on the configurational instability in mode I+III has not been studied in the literature.

We shall show here that a positive T^0_{xx} favors both pure mode I and mixed-mode I+III instabilities through formation of drifting perturbations of large wavelength; while a negative T^0_{xx} prevents instabilities in pure mode I, and does not have any impact on the onset of the faceting instability in mode I+III.

In contrast to the work of Leblond et al. (2011) where no length scale was involved, a non-zero non-singular stress T^0_{xx} yields a characteristic length $\mathcal{L}_{xx} = (K^0_{\rm I}/T^0_{xx})^2$ which can be compared to the wavelength $\ell_{\rm pert} = 2\pi/|k|$ of the perturbation in the direction of the crack front. Combined with the sign ϵ_{xx} of T^0_{xx}, the ratio of these two lengths sets the values of the growth rate $\mathrm{Re}(\lambda)$ and the drift angle α, for any mode mixity ratio $\rho^0 = K^0_{\rm III}/K^0_{\rm I}$. We show in Fig. 3 the values of $\mathrm{Re}(\lambda)/|k|$ and α versus the mode mixity ratio, for several values of the non-singular stress T^0_{xx} and a Poisson ratio $\nu = 0.3$.

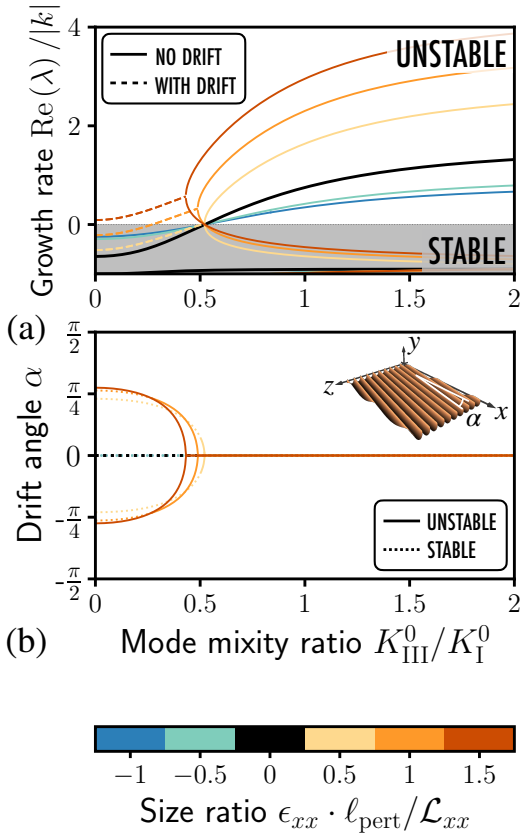

Figure 3: Configurational stability of a planar crack front for a Poisson ratio $\nu = 0.3$: influence of the non-singular stress T^0_{xx} on (a) the growth rate $\mathrm{Re}(\lambda)$ of the perturbation and (b) its drift angle α. The black curves correspond to the case $T^0_{xx} = 0$ considered by Leblond et al. (2011).

Prior to commenting on these results, a definition and some remarks are in order. We define $[K^0_{\rm III}/K^0_{\rm I}]_{\rm cr}$ as *the smallest value of the (non-negative) mixity ratio* $\rho^0 = K^0_{\rm III}/K^0_{\rm I}$ *for which the real part of the reduced growth rate* $\xi = \lambda/|k|$ *becomes non-negative*. It is important to note here that at the "threshold" $[K^0_{\rm III}/K^0_{\rm I}]_{\rm cr}$:

- $\mathrm{Re}(\xi)$ may be zero, *if* $[K^0_{\rm III}/K^0_{\rm I}]_{\rm cr}$ is positive; $\mathrm{Re}(\xi)$ then crosses the value 0 when $K^0_{\rm III}/K^0_{\rm I}$ crosses the value $[K^0_{\rm III}/K^0_{\rm I}]_{\rm cr}$;
- but $\mathrm{Re}(\xi)$ may also be positive, *if* $[K^0_{\rm III}/K^0_{\rm I}]_{\rm cr}$ is zero; $\mathrm{Re}(\xi)$ is then positive for all values of $K^0_{\rm III}/K^0_{\rm I}$;
- $\mathrm{Im}(\xi)$ need not necessarily be zero, and may take arbitrary values.

We observe in Fig. 3.a that negative non-singular stresses do not *qualitatively* change the stability behavior of the crack with respect to the reference case considered by Leblond et al. (2011): stability prevails for mode mixity ratios below $[K^0_{\rm III}/K^0_{\rm I}]_{\rm cr}$ and instability above it, and $[K^0_{\rm III}/K^0_{\rm I}]_{\rm cr}$ corresponds to the value $\xi = 0$ and is independent of T^0_{xx} - and thus remains equal to $[K^0_{\rm III}/K^0_{\rm I}]^{\rm ref}_{\rm cr}$. This means that a negative non-singular stress does not have any stabilizing influence on the onset of the mode I+III instability.

The case of a positive T_{xx} is also, and probably more, interesting: for low values of the mode mixity ratio, typically $K^0_{\rm III}/K^0_{\rm I} \lesssim 0.5$, drifting perturbations ($\alpha \neq 0$, dotted lines in Fig. 3.a) may develop along the crack surface, a feature that is absent for $T^0_{xx} = 0$. Note that both perturbations with a positive and a negative drift angle can form, owing to the invariance of the problem in a rotation of the geometry and loading of 180° around the x-axis (see Fig. 3.b). The critical value $[K^0_{\rm III}/K^0_{\rm I}]_{\rm cr}$ may also now depend on the non-singular stress T^0_{xx}. For low length scale ratios $\ell_{\rm pert}/\mathcal{L}_{xx} \lesssim 0.5$, the drifting perturbations decay in time ($\mathrm{Re}(\xi) < 0$), and exponentially growing, non-drifting perturbations ($\mathrm{Re}(\xi) > 0$, $\alpha = 0$) emerge when $K^0_{\rm III}/K^0_{\rm I}$ becomes larger than the value $[K^0_{\rm III}/K^0_{\rm I}]_{\rm cr} = [K^0_{\rm III}/K^0_{\rm I}]^{\rm ref}_{\rm cr}$, which still corresponds to $\xi = 0$ and remains independent of T^0_{xx} or $\ell_{\rm pert}/\mathcal{L}_{xx}$. For large length scale ratios $\ell_{\rm pert}/\mathcal{L}_{xx} \gtrsim 0.5$ (i.e. large values of T^0_{xx}), drifting perturbations emerge below the reference critical value $[K^0_{\rm III}/K^0_{\rm I}]^{\rm ref}_{\rm cr} \simeq 0.5$ obtained for $T^0_{xx} = 0$ (see Section 4.1). In other words, a large non-singular stress $T^0_{xx} > 0$ results in a *decrease* of the critical mode mixity $[K^0_{\rm III}/K^0_{\rm I}]_{\rm cr}$ for fragmentation. For even larger values of $\ell_{\rm pert}/\mathcal{L}_{xx}$, $[K^0_{\rm III}/K^0_{\rm I}]_{\rm cr}$ becomes zero so that perturbations grow even in the absence of mode III. These behaviors are qualitatively similar to those depicted by Cotterell and Rice (1980), Gao (1992) and Xu et al. (1994), who predicted that a positive T^0_{xx} favors out-of-plane crack excursions. Note that the behavior observed in Fig. 3 for large mode mixity ratios, $K^0_{\rm III}/K^0_{\rm I} \gtrsim 0.5$, is rather similar to that in the reference case $T^0_{xx} = 0$: out-of-plane perturbations grow in time, and propagate parallel to the mean direction of crack propagation ($\alpha = 0$), irrespective of the length scale ratio $\ell_{\rm pert}/\mathcal{L}_{xx}$.

The evolution of the critical mode mixity ratio $[K^0_{\rm III}/K^0_{\rm I}]_{\rm cr}$ - as defined above - with the length scale ratio $\epsilon_{xx}.\ell_{\rm pert}/\mathcal{L}_{xx}$ depends on Poisson's ratio, and is displayed in Fig. 4.a for $\nu \in [0.1, 0.5]$. Interestingly, as noted above, for all values of ν, above some "critical" length scale ratio $[\ell_{\rm pert}/\mathcal{L}_{xx}]_{\rm cr}$, $[K^0_{\rm III}/K^0_{\rm I}]_{\rm cr}$ becomes zero so that the perturbations grow exponentially no matter the mode mixity ratio. This critical length scale ratio is shown in Fig. 4.b and decreases almost linearly with Poisson's ratio, from about 1.87 to 0.77 for $\nu \in [0.1, 0.5]$. Unfortunately, no simple analytical expression of $[\ell_{\rm pert}/\mathcal{L}_{xx}]_{\rm cr}$ could be derived from Eq.(18). (The difficulty being that when $\epsilon_{xx}.\ell_{\rm pert}/\mathcal{L}_{xx} = [\ell_{\rm pert}/\mathcal{L}_{xx}]_{\rm cr}$, ξ is still not completely known since only its real part is zero).

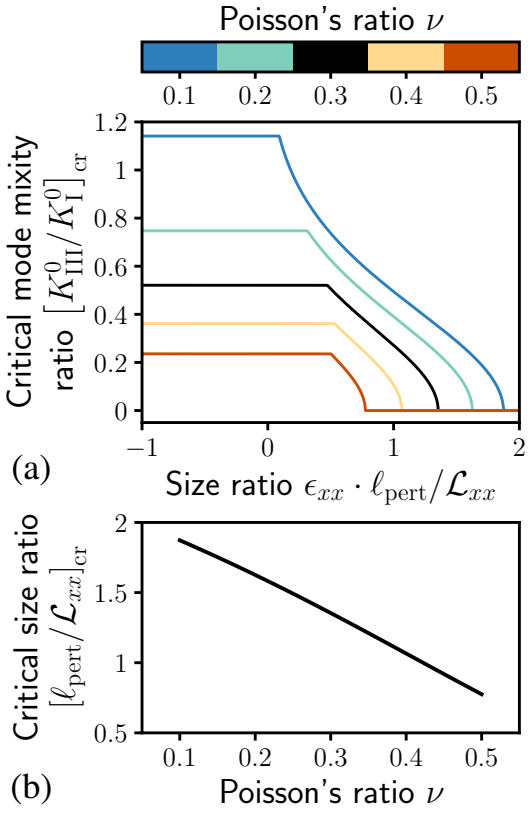

Figure 4: (a) Critical mode mixity ratio $[K^0_{\rm III}/K^0_{\rm I}]_{\rm cr}$ versus the perturbation size ratio $\epsilon_{xx}.\ell_{\rm pert}/\mathcal{L}_{xx}$, for various values of Poisson's ratio ν. (b) Evolution of the critical size ratio $[\ell_{\rm pert}/\mathcal{L}_{xx}]_{\rm cr}$ with Poisson's ratio ν. This is the perturbation size ratio for which the planar crack becomes unstable whatever the value of the mode mixity ratio $K^0_{\rm III}/K^0_{\rm I}$.

It should be noted that even though the existence of such a critical length scale ratio, above which instability prevails whatever the mixity ratio, is interesting, it cannot account for the small values of the mixity ratio at which facets form experimentally in some cases ($[K^0_{\rm III}/K^0_{\rm I}]_{\rm cr} \simeq 0.001 - 01$ for Homalite and PMMA, see Pham and Ravi-Chandar (2014) and Vasudevan (2018)). Indeed in these experiments, the non-singular stress T^0_{xx} was rather small, the length $\mathcal{L}_{xx}$ consequently rather large, so that the length scale ratio $\ell_{\rm pert}/\mathcal{L}_{xx}$ was *smaller* than the critical value $[\ell_{\rm pert}/\mathcal{L}_{xx}]_{\rm cr}$ - especially at the scale $\ell_{\rm pert} \simeq 10 - 100\,\mu$m at which the facets were observed.

Let us finally investigate the limiting 2D case, corresponding to perturbations independent of z, having thus a zero wavenumber k in the direction of the crack front. The reduced growth rate $\xi = \lambda/|k|$ then becomes ill-defined; but to solve this problem, it suffices to multiply Eq. (18) by $|k|$ and then let $|k|$ go to zero. One thus gets upon division by the common factor $\left[(1-\nu)(2-\nu) + (2+\nu)\rho_0^2\right]$:

$$\lambda - 2\sqrt{2\lambda}\frac{T^0_{xx}}{K^0_{\rm I}} = 0.$$

For a negative T^0_{xx}, this equation on λ does not have any solution, that is, there are no increasing perturbations (configurational stability). However, for $T^0_{xx} > 0$, it does admits a solution that reads:

$$\sqrt{\lambda} = 2\sqrt{2}\,\frac{T^0_{xx}}{K^0_{\rm I}} \quad \Rightarrow \quad \lambda = 8\left(\frac{T^0_{xx}}{K^0_{\rm I}}\right)^2 = 8\,\mathcal{L}_{xx}. \qquad (21)$$

We thus recover the results of Cotterell and Rice (1980), who showed that in 2D, the decreasing or increasing character of an arbitrary out-of-plane perturbation ϕ_y of the crack surface is controlled by the sole sign of T^0_{xx}. We also recover, for $T^0_{xx} > 0$, the value of the parameter λ governing the exponential growth of perturbations.

4.3. *Influence of* T^0_{zz}

We now investigate the influence of T^0_{zz} on the configurational stability of the planar crack. Like in the case where $T^0_{xx} \neq 0$, a non-zero non-singular stress T^0_{zz} yields a characteristic length $\mathcal{L}_{zz} = (K^0_{\rm I}/T^0_{zz})^2$ which may be compared to the perturbation wavelength $\ell_{\rm pert} = 2\pi/|k|$. Gao (1992) and Xu et al. (1994) showed that for pure mode I loading, the influence of T^0_{zz} on crack path stability is similar to that of T^0_{xx}: negative values of T^0_{zz} are associated to stable crack paths, while positive values favor instabilities. Moreover, Gao (1992) suggested that negative non-singular stresses T^0_{zz} may prevent the formation of *en echelon* cracking patterns associated to mixed mode I+III loadings.

We shall show here that negative non-singular stresses T^0_{zz} indeed stabilize out-of-plane perturbations in pure mode I, and significantly increase the mode mixity ratio at which the faceting (out-of-plane) instability may occur in mode I+III. In contrast, positive values of T^0_{zz} somehow favor both instabilities in pure mode I and mode I+III *for perturbations of large wavelength*, albeit in a less marked way than T^0_{xx}.

We show in Fig. 5 the normalized growth rate $\mathrm{Re}(\lambda)/|k|$ and the drift angle α as functions of the mode mixity ratio $\rho^0 = K^0_{\rm III}/K^0_{\rm I}$, for several values of the non-singular stress T^0_{zz} and a Poisson ratio $\nu = 0.3$. A general remark is that drifting perturbations ($\alpha \neq 0$) exist, but are of little interest since they always decrease in time. Negative non-singular stresses T^0_{zz} strongly stabilize the system, since even mode mixity ratios significantly larger than the reference threshold value $[K^0_{\rm III}/K^0_{\rm I}]^{\rm ref}_{\rm cr}$, corresponding to $T^0_{zz} = 0$, do not suffice to fragment the crack front. This is confirmed in Fig. 6.a, which shows $[K^0_{\rm III}/K^0_{\rm I}]_{\rm cr}$ - as defined in Subsection 4.2 above - as a function of the length scale ratio $\epsilon_{zz}.\ell_{\rm pert}/\mathcal{L}_{zz}$. Note that here $\mathrm{Im}(\xi)$ is always zero at the threshold ($K^0_{\rm III}/K^0_{\rm I} = [K^0_{\rm III}/K^0_{\rm I}]_{\rm cr}$). We observe that even a moderately negative non-singular stress T^0_{zz} triggers a significant increase of the critical mode mixity ratio, especially for low values of Poisson's ratio. Also, the positiveness of $[K^0_{\rm III}/K^0_{\rm I}]_{\rm cr}$ for all negative values of T^0_{zz} implies that such non-singular stresses preclude any out-of-plane instability in pure mode I (since $K^0_{\rm III}/K^0_{\rm I} = 0$ is then necessarily smaller than $[K^0_{\rm III}/K^0_{\rm I}]_{\rm cr} > 0$).

Positive non-singular stresses T^0_{zz} have an opposite impact upon stability of coplanar propagation, as they drive the system towards the mode I+III instability for lower critical mode mixity ratios $[K^0_{\rm III}/K^0_{\rm I}]_{\rm cr}$, see Fig. 5.a and Fig. 6.a. Like for the

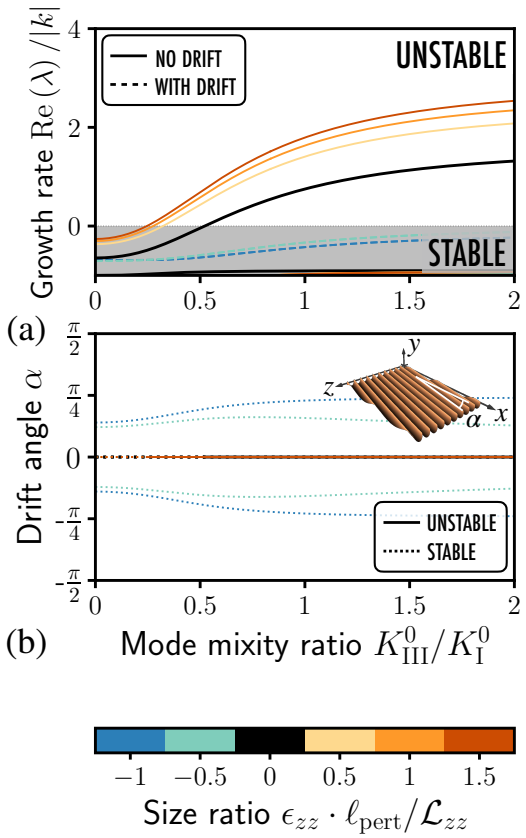

Figure 5: Configurational stability of a planar crack front for a Poisson ratio $\nu = 0.3$: influence of the non-singular stress T^0_{zz} on (a) the growth rate $\mathrm{Re}(\lambda)$ of the perturbation and (b) its drift angle α. The black curves correspond to the case $T^0_{zz} = 0$ considered by Leblond et al. (2011).

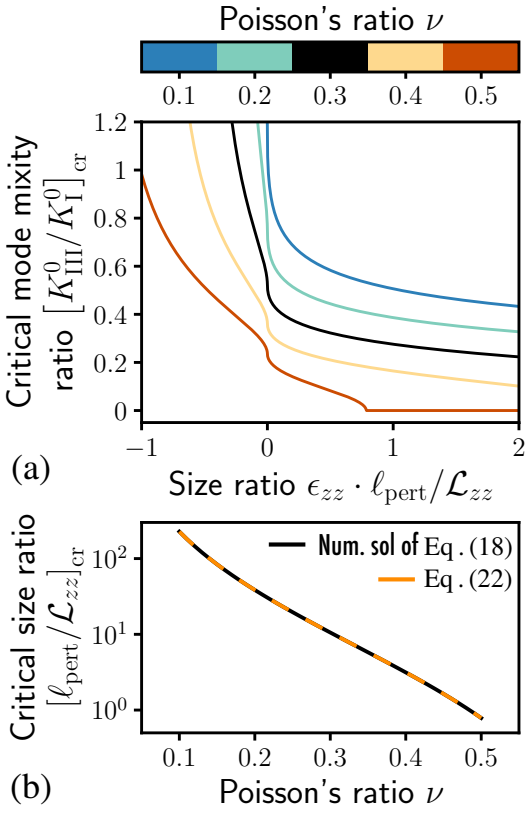

Figure 6: (a) Critical mode mixity ratio $[K^0_{\mathrm{III}}/K^0_{\mathrm{I}}]_{\mathrm{cr}}$ versus the perturbation size ratio $\epsilon_{zz}.\ell_{\mathrm{pert}}/\mathcal{L}_{zz}$, for various values of Poisson's ratio ν. (b) Evolution of the critical size ratio $[\ell_{\mathrm{pert}}/\mathcal{L}_{zz}]_{\mathrm{cr}}$ with Poisson's ratio ν. This is the perturbation size ratio for which the planar crack becomes unstable whatever the value of the mode mixity ratio $K^0_{\mathrm{III}}/K^0_{\mathrm{I}}$.

non-singular stress T^0_{xx}, we observe that there exists a critical length scale ratio $[\ell_{\mathrm{pert}}/\mathcal{L}_{zz}]_{\mathrm{cr}}$ above which $[K^0_{\mathrm{III}}/K^0_{\mathrm{I}}]_{\mathrm{cr}}$ becomes zero, so that perturbations grow unstably no matter the value of the mode mixity ratio. This means that *for a positive non-singular stress T^0_{zz}, large-wavelength perturbations increase in time even in pure mode I*. (In contrast, small-wavelength perturbations still decrease in time).

The critical length scale ratio $[\ell_{\mathrm{pert}}/\mathcal{L}_{zz}]_{\mathrm{cr}}$, above which coplanar propagation thus becomes unstable even in pure mode I, is determined by inserting the values $\rho_0 = K^0_{\mathrm{III}}/K^0_{\mathrm{I}} = 0$ and $\xi = 0$ (see Fig. 5.a) in Eq.(18); the result,

$$[\ell_{\mathrm{pert}}/\mathcal{L}_{zz}]_{\mathrm{cr}} = \frac{\pi}{4}\left(\frac{2-3\nu}{\nu}\right)^2 \qquad (22)$$

agrees with the values computed numerically (see Fig. 6.b). Equation (22) means that perturbations with a wavelength $\ell_{\mathrm{pert}} > \frac{\pi}{4}\left(\frac{2-3\nu}{\nu}\right)^2 \mathcal{L}_{zz}$ will grow in time. The $1/\nu^2$ dependence here accounts for the rapid decrease of $[\ell_{\mathrm{pert}}/\mathcal{L}_{zz}]_{\mathrm{cr}}$ with increasing values of ν: large values of Poisson's ratio favor crack front fragmentation, a behavior that is already clear in the absence of non-singular stresses, as the reference critical threshold ratio $[K^0_{\mathrm{III}}/K^0_{\mathrm{I}}]^{\mathrm{ref}}_{\mathrm{cr}}$ is also a decreasing function of ν (see Eq. 20). Note that the critical length scale ratio $[\ell_{\mathrm{pert}}/\mathcal{L}_{zz}]_{\mathrm{cr}}$ happens to be much larger than that, $[\ell_{\mathrm{pert}}/\mathcal{L}_{xx}]_{\mathrm{cr}}$, associated to the non-singular stress T^0_{xx}. This implies that the destabilizing effect of $T^0_{xx} > 0$ is much stronger than that of $T^0_{zz} > 0$.

Equation (22) is reminiscent of Eq. (21) that provides the growth rate of out-of-plane perturbations of a mode I 2D crack (invariant along the direction of the front), in the presence of some non-singular stress $T_{xx} > 0$. The formal similarity between both equations emphasizes the similarity between the phenomena they depict: *positive values of both non-singular stresses T^0_{xx} and T^0_{zz} imply, in pure mode I, formation of perturbations involving some characteristic length proportional to the square of $K^0_{\mathrm{I}}/T^0_{xx}$ or $K^0_{\mathrm{I}}/T^0_{zz}$*. In both cases this reflects the natural tendency of the crack to grow perpendicularly to the direction of far tensile principal stresses.

4.4. *Influence of T_{xz}*

Finally, we investigate the influence of the non-singular stress T^0_{xz} that introduces an additional length scale $\mathcal{L}_{xz} = (K^0_I/T^0_{xz})^2$ in the problem. Gao (1992) and Xu et al. (1994) found that it had no influence on crack path stability in pure mode I. Gao (1992) nonetheless suggested that even for such a loading, it may promote the formation of non-coplanar facets, due to the generation of a local mode III component if the crack

is slightly perturbed out of its original plane (see the third of Eqs. (A.9)).

We shall show here that a non-zero T^0_{xz} actually influences crack path stability in pure mode I, through formation of large-wavelength perturbations that drift along the front as the crack propagates. For mixed mode I+III loadings, the same mechanism also promotes the emergence of the faceting instability toward lower mode mixity ratios.

In Fig. 7, we display the normalized growth rate $\mathrm{Re}(\lambda)/|k|$ and the drift angle α as functions of the mode mixity ratio $\rho^0 = K^0_{\mathrm{III}}/K^0_{\mathrm{I}}$, for several values of the non-singular stress T^0_{xz} and a Poisson ratio $\nu = 0.3$. We observe that a non-zero T^0_{xz} may promote the formation of facets, as it lowers the value of the critical mode mixity ratio $[K^0_{\mathrm{III}}/K^0_{\mathrm{I}}]_{\mathrm{cr}}$ above which perturbations increase in time (see Fig. 7.a). This instability is characterized by a drifting motion of the crack front with a positive drift angle α when $T^0_{xz} < 0$, and a negative one when $T^0_{xz} > 0$ (see Fig. 7.b). Such an "oriented" drift of facets could somehow be anticipated, as the introduction of a non-zero T^0_{xz} breaks the invariance of the problem in a rotation of the geometry and loading of 180° about the x-axis.

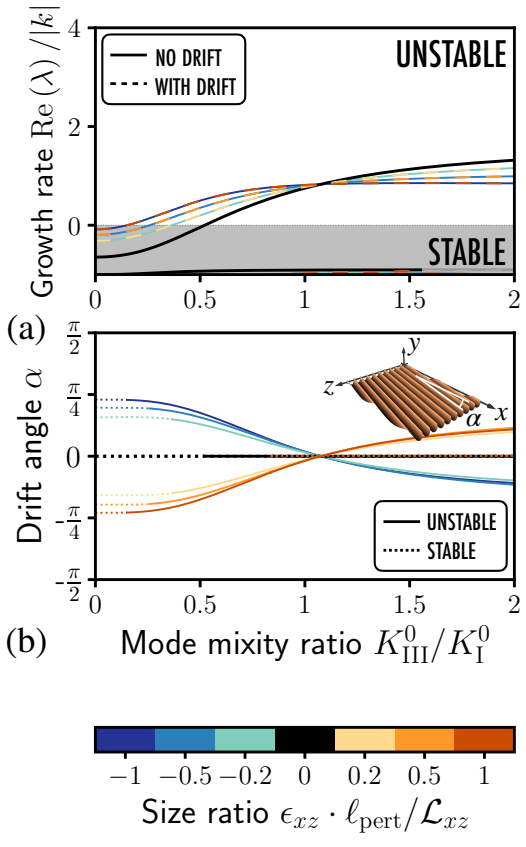

Figure 7: Configurational stability of a planar crack front for a Poisson ratio $\nu = 0.3$: influence of the non-singular stress T^0_{xz} on (a) the growth rate $\mathrm{Re}(\lambda)$ of the perturbation and (b) its drift angle α. The black curves correspond to the case $T^0_{xz} = 0$ considered by Leblond et al. (2011).

Figure 8 shows the critical mode mixity ratio $[K^0_{\mathrm{III}}/K^0_{\mathrm{I}}]_{\mathrm{cr}}$ as a function of the length scale ratio $\ell_{\mathrm{pert}}/\mathcal{L}_{xz}$. We observe a significant decrease of $[K^0_{\mathrm{III}}/K^0_{\mathrm{I}}]_{\mathrm{cr}}$ with increasing values of $|T^0_{xz}|$, especially for large Poisson ratios. It turns out that for small non-singular stresses T_{xz}, the critical ratio $[K^0_{\mathrm{III}}/K^0_{\mathrm{I}}]_{\mathrm{cr}}$ may be developed at first order in $q^0_{xz} \propto \sqrt{\ell_{\mathrm{pert}}/\mathcal{L}_{xz}}$, so that the threshold decreases linearly with $\sqrt{\ell_{\mathrm{pert}}/\mathcal{L}_{xz}}$; this explains the cusps on the vertical axis observed in Fig. 8. We again note, for each value of ν, the existence of a critical length scale ratio $[\ell_{\mathrm{pert}}/\mathcal{L}_{xz}]_{\mathrm{cr}}$ above which perturbations grow in time, even in pure mode I, no matter the sign of T^0_{xz}.

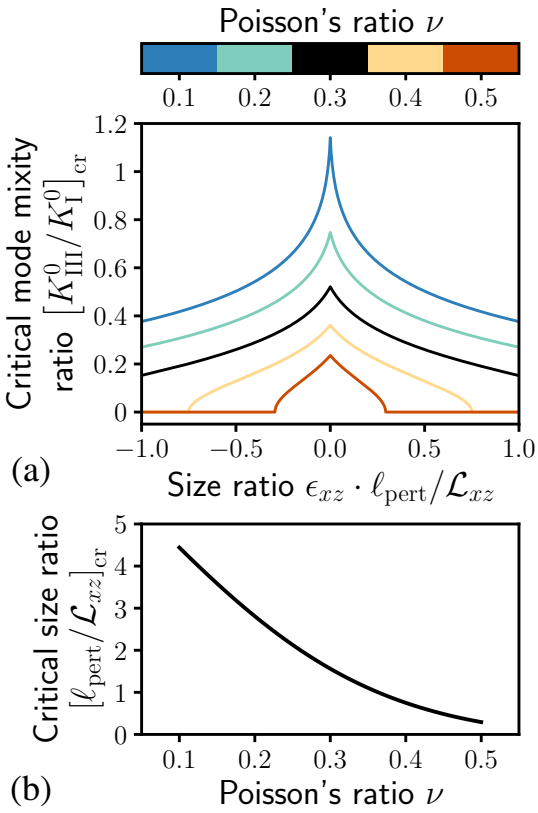

Figure 8: (a) Critical mode mixity ratio $[K^0_{\mathrm{III}}/K^0_{\mathrm{I}}]_{\mathrm{cr}}$ versus the perturbation size ratio $\epsilon_{xz}.\ell_{\mathrm{pert}}/\mathcal{L}_{xz}$, for various values of Poisson's ratio ν. (b) Evolution of the critical size ratio $[\ell_{\mathrm{pert}}/\mathcal{L}_{xz}]_{\mathrm{cr}}$ with Poisson's ratio ν. This is the perturbation size ratio for which the planar crack becomes unstable whatever the value of the mode mixity ratio $K^0_{\mathrm{III}}/K^0_{\mathrm{I}}$.

5. Conclusion

The configurational stability of a crack propagating under mixed-mode I+III loading conditions, with additional non-singular stresses T^0_{xx}, T^0_{zz}, T^0_{xz}, was investigated within the perturbative framework of linear elastic fracture mechanics, on the basis of a linear stability analysis. The work stood as a natural extension of that of Leblond et al. (2011), that did not account for the influence of non-singular stresses upon the onset of the faceting instability. We showed that the critical mode mixity ratio $[K^0_{\mathrm{III}}/K^0_{\mathrm{I}}]_{\mathrm{cr}}$, at which the instability emerges, is strongly influenced by the presence of non-singular stresses, due to the emergence of perturbations of large wavelength which may or may not drift along the front as the crack propagates. The

possibility evidenced here of a drifting motion of instability modes has been observed experimentally, see for example Lin et al. (2010) and Vasudevan (2018), and is similar to that predicted for a crack loaded under completely general mixed mode I+II+III conditions (Vasudevan et al., 2020).

More specifically, the main findings of this study are as follows:

- A negative non-singular stress T^0_{xx} does not promote formation of facets, and leaves unchanged the instability threshold $[K^0_{\mathrm{III}}/K^0_{\mathrm{I}}]_{\mathrm{cr}}$ which thus retains the value calculated by Leblond et al. (2011) in the absence of non-singular stresses. On the contrary, a positive non-singular stress T^0_{xx} lowers the critical mode mixity ratio $[K^0_{\mathrm{III}}/K^0_{\mathrm{I}}]_{\mathrm{cr}}$, through formation of drifting facets. The impact of a positive T^0_{xx} gets stronger as the ratio between the wavelength ℓ_{pert} of the perturbation approaches the structural length scale $\mathcal{L}_{xx} = (K^0_{\mathrm{I}}/T^0_{xx})^2$ associated to T^0_{xx}. For perturbations of large wavelength, or large values of T^0_{xx}, facets growing in time may even form no matter the value of the mixity ratio ($[K^0_{\mathrm{III}}/K^0_{\mathrm{I}}]_{\mathrm{cr}} = 0$).

- A negative non-singular stress T^0_{zz} strongly stabilizes straight crack fronts, as growing facets can only form for mode mixity ratios $K^0_{\mathrm{III}}/K^0_{\mathrm{I}}$ considerably larger than the instability threshold calculated by Leblond et al. (2011) in the absence of non-singular stresses. In contrast, a positive T^0_{zz} promotes the faceting instability, as the critical mode mixity ratio $[K^0_{\mathrm{III}}/K^0_{\mathrm{I}}]_{\mathrm{cr}}$ is a decreasing function of the length scale ratio $\ell_{\mathrm{pert}}/\mathcal{L}_{zz}$. Like for the non-singular stress T^0_{xx}, growing facets may even form no matter the mode mixity ratio, if $\ell_{\mathrm{pert}}/\mathcal{L}_{zz}$ is large enough. However the critical length scale ratio $[\ell_{\mathrm{pert}}/\mathcal{L}_{zz}]_{\mathrm{cr}}$, above which this phenomenon occurs, happens to be much larger than that, $[\ell_{\mathrm{pert}}/\mathcal{L}_{xx}]_{\mathrm{cr}}$, associated to the non-singular stress T^0_{xx}.

- Non-zero non-singular stresses T^0_{xz} promote the mode I+III instability, through formation of "oriented" facets that drift along the front in a specific direction determined by the sign of T^0_{xz}. Again, we also predict that facets may even form no matter the mode mixity ratio, if the length scale ratio $\ell_{\mathrm{pert}}/\mathcal{L}_{xz}$ is large enough.

The existence, for the ratios of the wavelength ℓ_{pert} of the perturbation and the structural length scales $\mathcal{L}_{xx}$, $\mathcal{L}_{zz}$, $\mathcal{L}_{xz}$, of critical values $[\ell_{\mathrm{pert}}/\mathcal{L}_{xx}]_{\mathrm{cr}}$, $[\ell_{\mathrm{pert}}/\mathcal{L}_{zz}]_{\mathrm{cr}}$, $[\ell_{\mathrm{pert}}/\mathcal{L}_{xz}]_{\mathrm{cr}}$ above which perturbations grow in time whatever the mode mixity ratio $K^0_{\mathrm{III}}/K^0_{\mathrm{I}}$, has important implications for the stability of crack path under *pure mode I loading* conditions. In two dimensions, Cotterell and Rice (1980) showed that crack path stability is controlled by the sole sign of T^0_{xx}. In three dimensions, the picture is more complex; the conclusions drawn from the present work can be summarized as follows:

- For negative non-singular stresses T^0_{xx} or T^0_{zz}, the system is stable versus perturbations of arbitrary wavelength in the direction of the crack front.

- For positive non-singular stresses T^0_{xx} or T^0_{zz}, and non-zero non-singular stresses T^0_{xz}, perturbations with wavelength smaller than some critical value set by the structural length scale $\mathcal{L}_{ij} = (K^0_{\mathrm{I}}/T^0_{ij})^2$ decrease in time, while perturbations with larger wavelength grow unstably.

The study presented in this paper also provides interesting clues on the influence of non-singular stresses on the onset of the mode I+III out-of-plane instability. The contributions of non-singular stresses cannot be neglected in numerical simulations or experiments, as they typically emerge from the finiteness of the crack dimensions with respect to the size of the embedding structure, and from boundary conditions. Yet, our results cannot claim to provide an explanation to the formation of non-coplanar facets at the very low mode mixity ratios often observed in experiments (Lin et al., 2010; Pham and Ravi-Chandar, 2014; Vasudevan, 2018; Kolvin et al., 2018); indeed, the wavelength of the instability modes evidenced in this work is comparable to the structural length scales $\mathcal{L}_{ij}$ – of the order of some centimeters –, while the formation of facets has been observed experimentally at scales as low as some tens of microns.

Online access to data

The Python script used to generate the figures and the associated data are available at https://doi.org/10.5281/zenodo.5994126.

Acknowledgments

The authors gratefully thank Prof. Alain Karma of Northeastern University, for suggesting the work expounded in this paper, and stimulating and fruitful discussions.

The paper is intended as a tribute to the work of Prof. Alexander B. Movchan of Liverpool University, and especially to his article (Movchan et al., 1998) dealing with the out-of-plane perturbation of a semi-infinite crack, which has proved of fundamental importance for the analysis of the out-of-plane instability of cracks loaded in mixed-mode I+III or I+II+III.

CRediT authorship contribution statement

Mathias Lebihain: Conceptualization, Formal analysis, Visualization, Software, Writing - Original Draft; **Jean-Baptiste Leblond:** Conceptualization, Methodology, Formal analysis, Writing - Review & Editing **Laurent Ponson:** Conceptualization, Writing - Review & Editing;

Appendix A. Expressions of the perturbed SIF $\delta K_{\rm p}$ in presence of mixed-mode I+III and non-singular stresses

In this Appendix, we provide the expressions of the perturbations of the SIFs arising from those parts of the initial (unperturbed) stress field tied to (i) the unperturbed SIFs $K_{\rm I}^0$, $K_{\rm III}^0$; (ii) the unperturbed non-singular stresses T_{xx}^0, T_{zz}^0, T_{xz}^0. These expressions are given at first order in the pair of perturbations (ϕ_x, ϕ_y) of the crack front and surface. The expressions of the terms pertaining to the SIFs $K_{\rm I}^0$, $K_{\rm III}^0$ were given for arbitrary perturbations ϕ_x, ϕ_y by Leblond et al. (2011), building on the work of Gao and Rice (1986) and Movchan et al. (1998); and we derive here the expressions of the terms pertaining to the non-singular stresses T_{xx}^0, T_{zz}^0, T_{xz}^0, with a comparison of the partial results of Movchan et al. (1998).

Appendix A.1. First-order perturbations of the stress intensity factors due to the initial stress intensity factors

At first order in the pair (ϕ_x, ϕ_y), the perturbations $\delta_K K_{\rm p}$ of the SIFs tied to the unperturbed SIFs $K_{\rm I}^0$, $K_{\rm III}^0$, consist of one contribution arising from the in-plane perturbation ϕ_x of the crack front, plus another one arising from the out-of-plane perturbation ϕ_y of the crack surface. According to the work of Gao and Rice (1986) for the in-plane perturbation, and those of Movchan et al. (1998) and Leblond et al. (2011) for the out-of-plane perturbation, the expressions of these perturbations read:

$$\begin{cases} \delta_K K_{\rm I}(x,z) = \dfrac{K_{\rm I}^0}{2\pi}\mathrm{PV}\displaystyle\int_{-\infty}^{+\infty}\frac{\phi_x(x,z')-\phi_x(x,z)}{(z-z')^2}dz' - 2K_{\rm III}^0\phi_{y,z}(x,z) + \delta K_{\rm I}^{\rm skew}(x,z) \\ \delta_K K_{\rm II}(x,z) = -\dfrac{2}{2-\nu}K_{\rm III}^0\phi_{x,z}(x,z) + \dfrac{K_{\rm I}^0}{2}\phi_{y,x}(x,z) - \dfrac{2-3\nu}{2-\nu}\dfrac{K_{\rm I}^0}{2\pi}\mathrm{PV}\displaystyle\int_{-\infty}^{+\infty}\frac{\phi_y(x,z')-\phi_y(x,z)}{(z-z')^2}dz' \\ \delta_K K_{\rm III}(x,z) = \dfrac{2+\nu}{2-\nu}\dfrac{K_{\rm III}^0}{2\pi}\mathrm{PV}\displaystyle\int_{-\infty}^{+\infty}\frac{\phi_x(x,z')-\phi_x(x,z)}{(z-z')^2}dz' + \dfrac{2(1-\nu)^2}{2-\nu}K_{\rm I}^0\phi_{y,z}(x,z) \end{cases} \tag{A.1}$$

where the symbol PV denotes a Cauchy principal value. The term $\delta K_{\rm I}^{\rm skew}$ in $\delta_K K_{\rm I}$ was calculated for an out-of-plane perturbation ϕ_y independent of x by Movchan et al. (1998), and in the general case by Leblond et al. (2011), with the following result:

$$\delta K_{\rm I}^{\rm skew}(x,z) = \frac{\sqrt{2}}{4\pi}\frac{1-2\nu}{1-\nu}K_{\rm III}^0\mathrm{Re}\left\{\int_{-\infty}^{x}dx'\int_{-\infty}^{+\infty}\frac{\phi_{y,x}(x',z')}{(x-x')^{1/2}\left[(x-x')+i(z-z')\right]^{3/2}}dz'\right\} \tag{A.2}$$

where the cut of the complex power function is along the half-line of non-positive real numbers. As explained in Section 2, expressions (A.1) and (A.2) disregard the influence of the spatial variations of the loading on the variations of the SIFs (because the lengths involved, of the order of $|(\partial K_{\rm p}^0/\partial x)/K_{\rm p}^0|$, are assumed to be much larger than the typical length over which the perturbations ϕ_x, ϕ_y vary significantly).

Appendix A.2. First-order perturbations of the stress intensity factors due to initial non-singular stresses

The calculation of the variations $\delta_T K_{\rm p}$ of the SIFs tied to the non-singular stresses T_{xx}^0, T_{zz}^0, T_{xz}^0 was presented in the work of Movchan et al. (1998). These variations were shown to depend only on the out-of-plane perturbation ϕ_y of the crack. They were calculated only for a perturbation ϕ_y independent of x and sinusoidal in z. Their expressions are derived here for an arbitrary ϕ_y. Some details on the derivation are given because of some discrepancies with the results of Movchan et al. (1998), see Appendix B below.

We first recall that according to Movchan et al. (1998)'s results, the variations of SIFs arising from the out-of-plane perturbation ϕ_y of the crack surface involve three kinds of terms: (i) *local* terms that relate to the local displacement of the front and orientation of the crack surface, characterized by the quantities ϕ_y, $\phi_{y,x}$, $\phi_{y,z}$; (ii) *semi-local* terms that involve integrals over the whole crack front of its displacement ϕ_y; and (iii) *non-local* terms in the form of integrals of ϕ_y extended over the entire crack surface. Furthermore we observe from the results derived in Section 3.5 of Movchan et al. (1998), that the variations $\delta_T K_{\rm p}$ involve only "morphology terms" (in the authors' terminology) which are of type (iii). It is thus possible to retrieve the expressions of these variations by considering a perturbation ϕ_y that leaves unchanged both the local position of the crack front and the local orientation of the crack surface at all points of the front ($\phi_y = 0$, $\phi_{y,x} = \phi_{y,z} = 0$ along the front): under such conditions other (local or semi-local) terms in the expressions of the variations of SIFs arising from the out-of-plane perturbation ϕ_y will vanish.

To determine the variations $\delta_T K_{\rm p}$ under such conditions, let us expand the solution $(\mathbf{u}, \boldsymbol{\sigma})$ of the elasticity problem at first order in the perturbation:

$$\begin{cases} \mathbf{u}(\mathbf{x}) = \mathbf{u}^0(\mathbf{x}) + \mathbf{u}^1(\mathbf{x}) \\ \boldsymbol{\sigma}(\mathbf{x}) = \boldsymbol{\sigma}^0(\mathbf{x}) + \boldsymbol{\sigma}^1(\mathbf{x}) \end{cases} \tag{A.3}$$

where the displacement and stress fields $\mathbf{u}^0$ and $\boldsymbol{\sigma}^0$ are of order 0, and the fields $\mathbf{u}^1$ and $\boldsymbol{\sigma}^1$ of order 1. *All four fields are defined on the unperturbed cracked body*: this is obvious for the fields $\mathbf{u}^0$ and $\boldsymbol{\sigma}^0$, and for the fields $\mathbf{u}^1$ and $\boldsymbol{\sigma}^1$ it stems from the fact that they correspond to the derivatives, on the unperturbed configuration, of the displacement and stress fields with respect to the amplitude

of the perturbation. We shall also need to expand the exterior normal vector $\mathbf{n}(x, y = \phi_y(x,z), z)$ to the perturbed crack surface in a similar way:

$$\mathbf{n}(x, \phi_y(x,z), z) = \mathbf{n}^0 + \mathbf{n}^1(x,z). \tag{A.4}$$

Let us now expand the condition of zero traction on the perturbed crack surface:

$$\begin{aligned}\mathbf{0} &= \boldsymbol{\sigma}(x, \phi_y(x,z), z).\mathbf{n}(x, \phi_y(x,z), z) = [\boldsymbol{\sigma}^0(x, \phi_y(x,z), z) + \boldsymbol{\sigma}^1(x, \phi_y(x,z), z)].[\mathbf{n}^0 + \mathbf{n}^1(x,z)] \\ &= \boldsymbol{\sigma}^0(x,0,z).\mathbf{n}^0 + \boldsymbol{\sigma}^0_{,y}(x,0,z).\mathbf{n}^0\phi_y(x,z) + \boldsymbol{\sigma}^0(x,0,z).\mathbf{n}^1(x,z) + \boldsymbol{\sigma}^1(x,0,z).\mathbf{n}^0.\end{aligned}$$

Identifying terms of order 1 in the perturbation in this equation, we get the boundary condition satisfied by the first-order fields on the unperturbed crack:

$$\boldsymbol{\sigma}^1(x,0,z).\mathbf{n}^0 = -\boldsymbol{\sigma}^0_{,y}(x,0,z).\mathbf{n}^0\phi_y(x,z) - \boldsymbol{\sigma}^0(x,0,z).\mathbf{n}^1(x,z) \equiv \mathbf{t}^{\text{eff}}(x,z). \tag{A.5}$$

We now develop this boundary condition in a more explicit form for those terms, in the unperturbed stress field $\boldsymbol{\sigma}^0$, which are connected to the non-singular stresses T^0_{xx}, T^0_{zz}, T^0_{xz}. First we note that for these terms, the gradient of $\boldsymbol{\sigma}^0$ is zero so that the term $-\boldsymbol{\sigma}^0_{,y}(x,0,z).\mathbf{n}^0\phi_y(x,z)$ in Eq. (A.5) vanishes. Second, we remark that the vectors $\mathbf{n}^0$ and $\mathbf{n}^1$ read, on the upper (+) and lower (-) unperturbed crack surfaces:

$$\left\{\begin{array}{lcl}\mathbf{n}^{0\pm} &=& \mp\mathbf{e}_y \\ \mathbf{n}^{1\pm}(x,z) &=& \pm\left(\phi_{y,x}(x,z)\mathbf{e}_x + \phi_{y,z}(x,z)\mathbf{e}_z\right).\end{array}\right. \tag{A.6}$$

Finally we remark that the terms pertaining to the non-singular stresses in the unperturbed stress field $\boldsymbol{\sigma}^0$ simply read

$$T^0_{xx}\mathbf{e}_x\otimes\mathbf{e}_x + T^0_{zz}\mathbf{e}_z\otimes\mathbf{e}_z + T^0_{xz}\left(\mathbf{e}_x\otimes\mathbf{e}_z + \mathbf{e}_z\otimes\mathbf{e}_x\right).$$

Using these elements, we get the "effective tractions" $\mathbf{t}^{\text{eff}}(x,z)$ appearing in the boundary condition (A.5) for the first-order solution on the upper and lower unperturbed crack surfaces:

$$\begin{array}{rcl}\boldsymbol{t}^{\text{eff}\,\pm}(x,z) &=& \boldsymbol{\sigma}^1(x,0,z).\mathbf{n}^{0\pm} \\ &=& -\boldsymbol{\sigma}^0(x,0,z).\mathbf{n}^{1\pm}(x,z) \\ &=& \mp\left[T^0_{xx}\mathbf{e}_x\otimes\mathbf{e}_x + T^0_{zz}\mathbf{e}_z\otimes\mathbf{e}_z + T^0_{xz}\left(\mathbf{e}_x\otimes\mathbf{e}_z + \mathbf{e}_z\otimes\mathbf{e}_x\right)\right]\cdot\left(\phi_{y,x}(x,z)\mathbf{e}_x + \phi_{y,z}(x,z)\mathbf{e}_z\right) \\ &=& \mp\left(T^0_{xx}\phi_{y,x}(x,z) + T^0_{xz}\phi_{y,z}(x,z)\right)\mathbf{e}_x \mp \left(T^0_{xz}\phi_{y,x}(x,z) + T^0_{zz}\phi_{y,z}(x,z)\right)\mathbf{e}_z.\end{array} \tag{A.7}$$

Now since the perturbation of the crack envisaged leaves unchanged the position of the crack front, the solution $(\mathbf{u}^1, \boldsymbol{\sigma}^1)$ possesses the usual $r^{-1/2}$ stress singularity near the front, which implies that it is a "classical" solution of bounded total energy, to which standard theorems of elasticity theory apply.[2] It follows that the p-th SIF at the point (x,z) of the unperturbed crack front, corresponding to this solution, is given in terms of Bueckner (1987) weight functions and the effective tractions by the integral

$$\int_{-\infty}^{x} dx' \int_{-\infty}^{+\infty} h_{\text{p}i}(x,z;x',z')t_i^{\text{eff}\,+}(x',z')dz' \tag{A.8}$$

where $h_{\text{p}i}(x,z;x',z')$, a *crack-face weight function*, is the p-th SIF generated at the point (x,z) of the front by a pair of opposite (equilibrated) unit forces applied in the directions $\pm\mathbf{e}_i$ at the points (x',z') of the unperturbed upper (+) and lower (-) crack surfaces. But since the perturbation envisaged also leaves unchanged the orientation of the crack surface, these SIFs on the unperturbed crack front simply coincide with those, $\delta_T K_{\text{p}}(x,z)$, arising from the unperturbed non-singular stresses in the perturbed solution.[3] It follows, using Eqs. (A.7) and (A.8) and the expressions of the crack-face weight functions for a semi-infinite crack in an infinite body, provided for instance in (Gao and Rice, 1986), that:

$$\left\{\begin{array}{lcl}\delta_T K_{\text{I}}(x,z) &=& 0 \\ \delta_T K_{\text{II}}(x,z) &=& -\dfrac{\sqrt{2}}{\pi^{3/2}}\displaystyle\int_{-\infty}^{x}dx'\int_{-\infty}^{+\infty}\frac{\sqrt{x-x'}}{(x-x')^2+(z-z')^2}\left[1+\frac{2\nu}{2-\nu}\frac{(x-x')^2-(z-z')^2}{(x-x')^2+(z-z')^2}\right]\left[T^0_{xx}\phi_{y,x}(x',z')+T^0_{xz}\phi_{y,z}(x',z')\right]dz' \\ && -\dfrac{\sqrt{2}}{\pi^{3/2}}\displaystyle\int_{-\infty}^{x}dx'\int_{-\infty}^{+\infty}\frac{\sqrt{x-x'}}{(x-x')^2+(z-z')^2}\frac{4\nu}{2-\nu}\frac{(x-x')(z-z')}{(x-x')^2+(z-z')^2}\left[T^0_{xz}\phi_{y,x}(x',z')+T^0_{zz}\phi_{y,z}(x',z')\right]dz' \\ \delta_T K_{\text{III}}(x,z) &=& -\dfrac{\sqrt{2}}{\pi^{3/2}}\displaystyle\int_{-\infty}^{x}dx'\int_{-\infty}^{+\infty}\frac{\sqrt{x-x'}}{(x-x')^2+(z-z')^2}\frac{4\nu}{2-\nu}\frac{(x-x')(z-z')}{(x-x')^2+(z-z')^2}\left[T^0_{xx}\phi_{y,x}(x',z')+T^0_{xz}\phi_{y,z}(x',z')\right]dz' \\ && -\dfrac{\sqrt{2}}{\pi^{3/2}}\displaystyle\int_{-\infty}^{x}dx'\int_{-\infty}^{+\infty}\frac{\sqrt{x-x'}}{(x-x')^2+(z-z')^2}\left[1-\frac{2\nu}{2-\nu}\frac{(x-x')^2-(z-z')^2}{(x-x')^2+(z-z')^2}\right]\left[T^0_{xz}\phi_{y,x}(x',z')+T^0_{zz}\phi_{y,z}(x',z')\right]dz'.\end{array}\right. \tag{A.9}$$

[2] *If* the perturbation implied a displacement of the front, the stress $\boldsymbol{\sigma}^1$ would behave near it like $r^{-3/2}$ so that the corresponding total energy would be infinite, implying a non-classical solution to which usual theorems would *not* apply.

[3] *If* the orientation of the surface was modified in the perturbation, the relation between these two sets of SIFs would involve additional terms tied to the small rotations $\phi_{y,x}$ and $\phi_{y,z}$ of this surface.

Appendix B. Expressions of the variations of the stress intensity factors using Fourier transforms

In this Appendix, we provide the expressions of the variations $\delta K_{\rm p}$ of the SIFs for the perturbations defined in Eq. (5), using the Fourier transforms $\hat{\psi}_x, \hat{\psi}_y$ of the functions ψ_x, ψ_y.

It is assumed below that $\mathrm{Re}(\xi) > -1$ or equivalently $\mathrm{Re}(\lambda) > -|k|$ (which is true for all values of the wavenumber k if $\mathrm{Re}(\lambda) > 0$); this condition is indeed required for convergence of the integrals obtained from the general expressions (A.1) of $\delta_K K_{\rm p}$ and (A.9) of $\delta_T K_{\rm p}$.

Appendix B.1. Variations of the stress intensity factors tied to $K^0_{\rm I}$, $K^0_{\rm III}$

For perturbations of the form (5), the expression of the variations $\delta_K K_{\rm p}$ of Eq. (A.1) are given by Leblond et al. (2019) as:

$$\begin{cases} \delta_K K_{\rm I}(x,z) &= \mathrm{Re}\left\{ e^{\lambda x} \int_{-\infty}^{+\infty} \left[-K^0_{\rm I} \frac{|k|}{2} \hat{\psi}_x(k) - i K^0_{\rm III} \left(2 - \frac{1-2\nu}{\sqrt{2}(1-\nu)} \frac{\lambda}{(\lambda+|k|)^{1/2}} \right) \hat{\psi}_y(k) \right] e^{ikz} dk \right\} \\ \delta_K K_{\rm II}(x,z) &= \mathrm{Re}\left\{ e^{\lambda x} \int_{-\infty}^{+\infty} \left[-i K^0_{\rm III} \frac{2}{2-\nu} k \hat{\psi}_x(k) + K^0_{\rm I} \left(\frac{\lambda}{2} + \frac{2-3\nu}{2(2-\nu)} |k| \right) \hat{\psi}_y(k) \right] e^{ikz} dk \right\} \\ \delta_K K_{\rm III}(x,z) &= \mathrm{Re}\left\{ e^{\lambda x} \int_{-\infty}^{+\infty} \left[-K^0_{\rm III} \frac{2+\nu}{2(2-\nu)} |k| \hat{\psi}_x(k) + i K^0_{\rm I} \frac{2(1-\nu)^2}{2-\nu} k \hat{\psi}_y(k) \right] e^{ikz} dk \right\} \end{cases} \tag{B.1}$$

Appendix B.2. Variations of the stress intensity factors tied to T^0_{xx}, T^0_{zz}, T^0_{xz}

We provide here the expressions of the variations $\delta_T K_{\rm p}$ of Eq. (A.9) for perturbations of the form (5). As an example of the kind of calculations required, here are those necessary to evaluate the first integral, $\delta^1_T K_{\rm II}$, appearing in the expression $(\mathrm{A.9})_2$ of $\delta_T K_{\rm II}$:

$$\begin{aligned} \delta^1_T K_{\rm II}(x,z) &= -\frac{\sqrt{2}}{\pi^{3/2}} \int_{-\infty}^{x} dx' \int_{-\infty}^{+\infty} \frac{\sqrt{x-x'}}{(x-x')^2+(z-z')^2} \left[1 + \frac{2\nu}{2-\nu} \frac{(x-x')^2-(z-z')^2}{(x-x')^2+(z-z')^2} \right] \left[T^0_{xx} \phi_{y,x}(x',z') + T^0_{xz} \phi_{y,z}(x',z') \right] dz' \\ &= -\frac{\sqrt{2}}{\pi^{3/2}} \mathrm{Re}\left\{ \int_{-\infty}^{x} e^{\lambda x'} dx' \int_{-\infty}^{+\infty} \frac{\sqrt{x-x'}}{(x-x')^2+(z-z')^2} \left[1 + \frac{2\nu}{2-\nu} \frac{(x-x')^2-(z-z')^2}{(x-x')^2+(z-z')^2} \right] \left[\lambda T^0_{xx} \psi_y(z') + T^0_{xz} \psi_{y,z}(z') \right] dz' \right\} \\ &= -\frac{\sqrt{2}}{\pi^{3/2}} \mathrm{Re}\left\{ \int_{-\infty}^{x} e^{\lambda x'} dx' \int_{-\infty}^{+\infty} \frac{\sqrt{x-x'}}{(x-x')^2+(z-z')^2} \left[1 + \frac{2\nu}{2-\nu} \frac{(x-x')^2-(z-z')^2}{(x-x')^2+(z-z')^2} \right] dz' \int_{-\infty}^{+\infty} \left(\lambda T^0_{xx} + ikT^0_{xz} \right) \hat{\psi}_y(k) e^{ikz'} dk \right\} \\ &= -\frac{\sqrt{2}}{\pi^{3/2}} \mathrm{Re}\left\{ \int_{-\infty}^{x} e^{\lambda x'} dx' \int_{-\infty}^{+\infty} \frac{\sqrt{x-x'}}{(x-x')^2+(z-z')^2} \left[\frac{2-3\nu}{2-\nu} + \frac{4\nu}{2-\nu} \frac{(x-x')^2}{(x-x')^2+(z-z')^2} \right] dz' \int_{-\infty}^{+\infty} \left(\lambda T^0_{xx} + ikT^0_{xz} \right) \hat{\psi}_y(k) e^{ikz'} dk \right\} \\ \underset{\substack{u=x-x' \\ v=z-z'}}{\longrightarrow} &= -\frac{\sqrt{2}}{\pi^{3/2}(2-\nu)} \mathrm{Re}\left\{ e^{\lambda x} \int_{-\infty}^{+\infty} \left(\lambda T^0_{xx} + ikT^0_{xz} \right) \hat{\psi}_y(k) e^{ikz} dk \int_0^{+\infty} \sqrt{u}\, e^{-\lambda u} du \int_{-\infty}^{+\infty} \left[\frac{2-3\nu}{u^2+v^2} + 4\nu \frac{u^2}{(u^2+v^2)^2} \right] e^{-ikv} dv \right\} \\ &= -\frac{\sqrt{2}}{\pi^{3/2}(2-\nu)} \mathrm{Re}\left\{ e^{\lambda x} \int_{-\infty}^{+\infty} \left(\lambda T^0_{xx} + ikT^0_{xz} \right) \hat{\psi}_y(k) e^{ikz} dk \int_0^{+\infty} \pi \frac{e^{-(\lambda+|k|)u}}{\sqrt{u}} \left[2 - 3\nu + 2\nu(1+|k|u) \right] du \right\} \\ &= -\sqrt{2}\, \mathrm{Re}\left\{ e^{\lambda x} \int_{-\infty}^{+\infty} \left(\lambda T^0_{xx} + ikT^0_{xz} \right) \left[\frac{1}{(\lambda+|k|)^{1/2}} + \frac{\nu}{2-\nu} \frac{|k|}{(\lambda+|k|)^{3/2}} \right] \hat{\psi}_y(k) e^{ikz} dk \right\}. \end{aligned} \tag{B.2}$$

The last steps of the calculation here used the following results (see formulae (3.723.2), (3.729.1) and (3.944.6) of Gradshteyn and Ryzhik (2014)):

$$\begin{cases} \displaystyle\int_{-\infty}^{+\infty} \frac{e^{-ikv}}{u^2+v^2} dv = \frac{\pi}{u} e^{-|k|u} \quad ; \quad \int_{-\infty}^{+\infty} \frac{e^{-ikv}}{(u^2+v^2)^2} dv = \frac{\pi}{2u^3} (1+|k|u) e^{-|k|u} \\ \displaystyle\int_{-\infty}^{+\infty} \frac{e^{-(\lambda+|k|)u}}{\sqrt{u}} du = \sqrt{\pi} (\lambda+|k|)^{-1/2} \quad ; \quad \int_{-\infty}^{+\infty} \sqrt{u}\, e^{-(\lambda+|k|)u} du = \frac{\sqrt{\pi}}{2} (\lambda+|k|)^{-3/2}. \end{cases} \tag{B.3}$$

The three remaining integrals of Eq. (A.9) may be calculated in a similar way, using in addition formula (3.729.2) of Gradshteyn and Ryzhik (2014). The final results read as follows:

$$\begin{cases} \delta_T K_{\rm I}(x,z) &= 0 \\ \delta_T K_{\rm II}(x,z) &= \sqrt{2}\, \mathrm{Re}\left\{ e^{\lambda x} \int_{-\infty}^{+\infty} \left[-\left(1 + \frac{\nu}{2-\nu} \frac{|k|}{\lambda+|k|} \right) \frac{\lambda}{(\lambda+|k|)^{1/2}} T^0_{xx} - \frac{\nu}{2-\nu} \frac{k^2}{(\lambda+|k|)^{3/2}} T^0_{zz} - i \left(1 - \frac{\nu}{2-\nu} \frac{\lambda-|k|}{\lambda+|k|} \right) \frac{k}{(\lambda+|k|)^{1/2}} T^0_{xz} \right] \hat{\psi}_y(k) e^{ikz} dk \right\} \\ \delta_T K_{\rm III}(x,z) &= \sqrt{2}\, \mathrm{Re}\left\{ e^{\lambda x} \int_{-\infty}^{+\infty} \left[i \frac{\nu}{2-\nu} \frac{\lambda k}{(\lambda+|k|)^{3/2}} T^0_{xx} - i \left(1 - \frac{\nu}{2-\nu} \frac{|k|}{\lambda+|k|} \right) \frac{k}{(\lambda+|k|)^{1/2}} T^0_{zz} - \left(\lambda - \frac{\nu}{2-\nu} \frac{\lambda-|k|}{\lambda+|k|} |k| \right) \frac{1}{(\lambda+|k|)^{1/2}} T^0_{xz} \right] \hat{\psi}_y(k) e^{ikz} dk \right\}. \end{cases} \tag{B.4}$$

For the sinusoidal perturbation independent of x considered by Gao (1992) and Movchan et al. (1998), $\phi_y(z) = A\cos(kz)$, $k > 0$ (that is, $\lambda = 0$ and $\hat{\psi}_y(k') = \frac{A}{2}[\delta(k'-k) + \delta(k'+k)]$), one thus gets:

$$\begin{cases} \delta_T K_{\mathrm{II}}(z) = A\dfrac{\sqrt{2k}}{2-\nu}\left[2T^0_{xz}\sin(kz) - \nu T^0_{zz}\cos(kz)\right] \\ \delta_T K_{\mathrm{III}}(z) = A\dfrac{\sqrt{2k}}{2-\nu}\left[-\nu T^0_{xz}\cos(kz) + 2(1-\nu)T^0_{zz}\sin(kz)\right]. \end{cases} \tag{B.5}$$

These expressions agree with Eqs (40) and (41) of Gao (1992).[4] When comparing our results to Eqs. (3.44) and (3.45) of Movchan et al. (1998), however, we note sign discrepancies in the term proportional to T^0_{zz} in the expression of $\delta_T K_{\mathrm{II}}$, and in the term proportional to T^0_{xz} in the expression of $\delta_T K_{\mathrm{III}}$. It is unfortunately not possible to check Movchan et al. (1998)'s calculations because they are not detailed in their paper.

Appendix C. Procedure of solution of Eq. (18)

The study of general (complex) solutions in ξ of Eq. (18) is made easier by adopting the change of variable suggested by Leblond et al. (2011):

$$\zeta = \frac{1}{\sqrt{\xi+1}} \quad \Leftrightarrow \quad \xi = \frac{1}{\zeta^2} - 1 \quad (\text{with } \mathrm{Re}(\xi) > -1 \;\Leftrightarrow\; |\mathrm{Arg}(\zeta)| < \frac{\pi}{4}). \tag{C.1}$$

Equation (18) reduces, after some manipulations, to the following algebraic equation of the 5th degree in ζ:

$$\begin{aligned} &2\sqrt{2}\nu\left(\rho_0^2 - (1+\nu)\right)\left[q^0_{xx} - 2isq^0_{xz} - q^0_{zz}\right]\zeta^5 + 4\sqrt{2}\left[-(1-2\nu)\rho_0^2 - \left((1+\nu)\rho_0^2 + (1-\nu)^2\right)q^0_{xx} + \left((3+\nu)\rho_0^2 + (1-\nu)^2\right)isq^0_{xz} + 2\rho_0^2 q^0_{zz}\right]\zeta^3 \\ &+ \left[2(4-\nu)\rho_0^2 + 2\nu(1-\nu)\right]\zeta^2 + 2\sqrt{2}\left[\left((2+\nu)\rho_0^2 + (1-\nu)(2-\nu)\right)q^0_{xx} - 4\rho_0^2 isq^0_{xz}\right]\zeta - (2+\nu)\rho_0^2 - (1-\nu)(2-\nu) = 0. \end{aligned} \tag{C.2}$$

The roots of Eq. (C.2) are calculated numerically using the function `roots` of the Python library Numpy (Harris et al., 2020). The method relies on evaluation of the eigenvalues of the companion matrix. Only the roots satisfying the condition $|\mathrm{Arg}(\zeta)| < \pi/4$ are of interest, so that the number of retained roots may be less than 5.

References

Baumberger, T., Caroli, C., Martina, D., Ronsin, O., 2008. Magic angles and cross-hatching instability in hydrogel fracture. Physical Review Letters 100, 178303. URL: https://link.aps.org/doi/10.1103/PhysRevLett.100.178303, doi:10.1103/PhysRevLett.100.178303.

Bueckner, H., 1987. Weight functions and fundamental fields for the penny-shaped and the half-plane crack in three-space. International Journal of Solids and Structures 23, 57–93. URL: http://www.sciencedirect.com/science/article/pii/0020768387900321, doi:10.1016/0020-7683(87)90032-1.

Chen, C.H., Cambonie, T., Lazarus, V., Nicoli, M., Pons, A.J., Karma, A., 2015. Crack front segmentation and facet coarsening in mixed-mode fracture. Physical Review Letters 115, 265503. URL: https://link.aps.org/doi/10.1103/PhysRevLett.115.265503, doi:10.1103/PhysRevLett.115.265503.

Cotterell, B., Rice, J., 1980. Slightly curved or kinked cracks. International Journal of Fracture 16, 155–169. URL: https://doi.org/10.1007/BF00012619, doi:10.1007/BF00012619.

Eberlein, A., Richard, H.A., Kullmer, G., 2017. Facet formation at the crack front under combined crack opening and anti-plane shear loading. Engineering Fracture Mechanics 174, 21–29. URL: https://www.sciencedirect.com/science/article/pii/S0013794416307354, doi:10.1016/j.engfracmech.2016.12.004.

Favier, E., Lazarus, V., Leblond, J.B., 2006. Statistics of the deformation of the front of a tunnel-crack propagating in some inhomogeneous medium. Journal of the Mechanics and Physics of Solids 54, 1449–1478. URL: http://www.sciencedirect.com/science/article/pii/S0022509606000160, doi:10.1016/j.jmps.2006.01.004.

Gao, H., 1992. Three-dimensional slightly nonplanar cracks. Journal of Applied Mechanics 59, 335–343. URL: https://doi.org/10.1115/1.2899525, doi:10.1115/1.2899525.

Gao, H., Rice, J., 1986. Shear stress intensity factors for a planar crack with slightly curved front. Journal of Applied Mechanics 53, 774–778. URL: http://dx.doi.org/10.1115/1.3171857, doi:10.1115/1.3171857.

Goldstein, R.V., Salganik, R.L., 1974. Brittle fracture of solids with arbitrary cracks. International Journal of Fracture 10, 507–523. URL: https://doi.org/10.1007/BF00155254, doi:10.1007/BF00155254.

Gradshteyn, I.S., Ryzhik, I.M., 2014. Table of integrals, series, and products. Seventh ed., Elsevier/Academic Press, Amsterdam.

Griffith, A., 1921. The phenomena of rupture and flow in solids. Phil. Trans. R. Soc. Lond. A 221. URL: http://rsta.royalsocietypublishing.org/content/221/582-593/163, doi:10.1098/rsta.1921.0006.

Harris, C.R., Millman, K.J., van der Walt, S.J., Gommers, R., Virtanen, P., Cournapeau, D., Wieser, E., Taylor, J., Berg, S., Smith, N.J., Kern, R., Picus, M., Hoyer, S., van Kerkwijk, M.H., Brett, M., Haldane, A., del Río, J.F., Wiebe, M., Peterson, P., Gérard-Marchant, P., Sheppard, K., Reddy, T., Weckesser, W., Abbasi, H., Gohlke, C., Oliphant, T.E., 2020. Array programming with NumPy. Nature 585, 357–362. URL: https://doi.org/10.1038/s41586-020-2649-2, doi:10.1038/s41586-020-2649-2.

Hourlier, F., Pineau, A., 1979. Fissuration par fatigue sous sollicitations polymodales (mode I ondulé + mode III permanent) d'un acier pour rotors 26ncdv14. Mem. Sci. Rev. Metall. 76, 175–185.

[4] They do not agree with Eq. (44) of (Gao, 1992), but the origin of the discrepancy can easily be traced back to a trivial typographic or algebraic error in the transition from his Eqs. (40) and (41) to his Eq. (44).

Irwin, G., 1958. Fracture, in: Flügge, S. (Ed.), Elasticity and Plasticity / Elastizität und Plastizittät. Springer Berlin Heidelberg. Handbuch der Physik / Encyclopedia of Physics, pp. 551–590. URL: https://doi.org/10.1007/978-3-642-45887-3.

Kermode, J.R., Albaret, T., Sherman, D., Bernstein, N., Gumbsch, P., Payne, M.C., Csányi, G., De Vita, A., 2008. Low-speed fracture instabilities in a brittle crystal. Nature 455, 1224–1227. URL: https://www.nature.com/articles/nature07297, doi:10.1038/nature07297.

Knauss, W.G., 1970. An observation of crack propagation in anti-plane shear. International Journal of Fracture Mechanics 6, 183–187. URL: https://doi.org/10.1007/BF00189825, doi:10.1007/BF00189825.

Kolvin, I., Cohen, G., Fineberg, J., 2018. Topological defects govern crack front motion and facet formation on broken surfaces. Nature Materials 17, 140–144. URL: https://www.nature.com/articles/nmat5008, doi:10.1038/nmat5008.

Lazarus, V., Buchholz, F.G., Fulland, M., Wiebesiek, J., 2008. Comparison of predictions by mode II or mode III criteria on crack front twisting in three or four point bending experiments. International Journal of Fracture 153, 141–151. URL: https://doi.org/10.1007/s10704-008-9307-2, doi:10.1007/s10704-008-9307-2.

Leblond, J., Karma, A., Lazarus, V., 2011. Theoretical analysis of crack front instability in mode i+III. Journal of the Mechanics and Physics of Solids 59, 1872–1887. URL: http://www.sciencedirect.com/science/article/pii/S0022509611001141, doi:10.1016/j.jmps.2011.05.011.

Leblond, J., Karma, A., Ponson, L., Vasudevan, A., 2019. Configurational stability of a crack propagating in a material with mode-dependent fracture energy - part i: Mixed-mode i+III. Journal of the Mechanics and Physics of Solids 126, 187–203. URL: http://www.sciencedirect.com/science/article/pii/S0022509618310184, doi:10.1016/j.jmps.2019.02.007.

Lin, B., Mear, M.E., Ravi-Chandar, K., 2010. Criterion for initiation of cracks under mixed-mode i + III loading. International Journal of Fracture 165, 175–188. URL: https://doi.org/10.1007/s10704-010-9476-7, doi:10.1007/s10704-010-9476-7.

Movchan, A., Gao, H., Willis, J., 1998. On perturbations of plane cracks. International Journal of Solids and Structures 35, 3419–3453. URL: http://www.sciencedirect.com/science/article/pii/S002076839700231X, doi:10.1016/S0020-7683(97)00231-X.

Pham, K.H., Ravi-Chandar, K., 2014. Further examination of the criterion for crack initiation under mixed-mode i+III loading. International Journal of Fracture 189, 121–138. URL: https://doi.org/10.1007/s10704-014-9966-0, doi:10.1007/s10704-014-9966-0.

Pollard, D.D., Segall, P., Delaney, P.T., 1982. Formation and interpretation of dilatant echelon cracks. GSA Bulletin 93, 1291–1303. URL: https://doi.org/10.1130/0016-7606(1982)93<1291:FAIODE>2.0.CO;2, doi:10.1130/0016-7606(1982)93¡1291:FAIODE¿2.0.CO;2.

Pons, A.J., Karma, A., 2010. Helical crack-front instability in mixed-mode fracture. Nature 464, 85–89. URL: https://www.nature.com/articles/nature08862, doi:10.1038/nature08862.

Ronsin, O., Caroli, C., Baumberger, T., 2014. Crack front échelon instability in mixed mode fracture of a strongly nonlinear elastic solid. EPL (Europhysics Letters) 105, 34001. URL: https://doi.org/10.1209/0295-5075/105/34001, doi:10.1209/0295-5075/105/34001.

Sommer, E., 1969. Formation of fracture 'lances' in glass. Engineering Fracture Mechanics 1, 539–546. URL: https://www.sciencedirect.com/science/article/pii/0013794469900101, doi:10.1016/0013-7944(69)90010-1.

Vasoya, M., Lazarus, V., Ponson, L., 2016. Bridging micro to macroscale fracture properties in highly heterogeneous brittle solids: weak pinning versus fingering. Journal of the Mechanics and Physics of Solids 95, 755–773. URL: http://www.sciencedirect.com/science/article/pii/S0022509615303604, doi:10.1016/j.jmps.2016.04.022.

Vasudevan, A., 2018. Deciphering triangular fracture patterns in PMMA : how crack fragments in mixed mode loading. Ph.D. thesis. Sorbonne Université. Paris. URL: https://tel.archives-ouvertes.fr/tel-02180510.

Vasudevan, A., Ponson, L., Karma, A., Leblond, J.B., 2020. Configurational stability of a crack propagating in a material with mode-dependent fracture energy – part II: Drift of fracture facets in mixed-mode i+II+III. Journal of the Mechanics and Physics of Solids 137, 103894. URL: http://www.sciencedirect.com/science/article/pii/S0022509619308865, doi:10.1016/j.jmps.2020.103894.

Wang, M., Adda-Bedia, M., Kolinski, J.M., Fineberg, J., 2022. How hidden 3d structure within crack fronts reveals energy balance. arXiv:2201.09939 [cond-mat] URL: http://arxiv.org/abs/2201.09939, arXiv:2201.09939.

Williams, M.L., 1952. Stress singularities resulting from various boundary conditions in angular corners of plates in extension. Journal of Applied Mechanics 19, 526–528. URL: http://resolver.caltech.edu/CaltechAUTHORS:20140730-111744170.

Xu, G., Bower, A.F., Ortiz, M., 1994. An analysis of non-planar crack growth under mixed mode loading. International Journal of Solids and Structures 31, 2167–2193. URL: https://www.sciencedirect.com/science/article/pii/0020768394902054, doi:10.1016/0020-7683(94)90205-4.